SIAM J. SCI. COMPUT.
Vol. 38, No. 1, pp. A346–A375

ATOMISTIC/CONTINUUM BLENDING WITH GHOST FORCE CORRECTION*

CHRISTOPH ORTNER† AND LEI ZHANG‡

Abstract. We combine the ideas of atomistic/continuum energy blending and ghost force correction to obtain an energy-based atomistic/continuum coupling scheme which has, for a range of benchmark problems, the same convergence rates as optimal force-based coupling schemes. We present the construction of this new scheme, numerical results exploring its accuracy in comparison with established schemes, and a rigorous error analysis for an instructive special case.

Key words. atomistic models, coarse graining, atomistic-to-continuum coupling, quasi-continuum method, blending

AMS subject classifications. 65N12, 65N15, 70C20, 82D25

DOI. 10.1137/15M1020241

1. Introduction.

Atomistic/continuum (a/c) coupling schemes are a popular class of multiscale methods for concurrent coupling between atomistic and continuum mechanics in the simulation of crystalline solids. An ongoing effort to develop a rigorous numerical analysis, summarized in [13], has led to a distillation of many key ideas in the field and a number of improvements.

It remains an open problem to construct a general and practical quasi-nonlocal (QNL)-type a/c coupling scheme along the lines of [25, 6, 23]. We propose that the present paper renders this search irrelevant, in that we construct an *energy-based* a/c coupling scheme with more superior rates of convergence (in our model problems) than a hypothetical QNL-type scheme would have. We achieve this by combining two popular ideas: ghost force correction [24] and blending [27].

In the ghost force correction method of Shenoy et al. [24] the spurious interface forces caused by a/c coupling (usually termed *ghost forces*) are removed by adding a suitable dead load correction, which can be computed either from a previous step in a quasi-static process or through a self-consistent iteration. In the latter case, this process was shown to be formally equivalent to the force-based quasi-continuum (QCF) scheme [4]. Difficult open problems remain in the analysis of the QCF method; see [12, 5, 11, 15] for recent advances. However, in practice the scheme seems to be optimal (in terms of the error committed by the coupling mechanism). The main drawback is that the QCF forces are nonconservative, i.e., there is no associated energy functional.

An alternative scheme to reduce the effect of ghost forces is the blending method of Xiao and Belytschko [27]. Instead of a sharp a/c interface, the atomistic and

*Submitted to the journal's Methods and Algorithms for Scientific Computing section May 6, 2015; accepted for publication (in revised form) November 9, 2015; published electronically February 2, 2016.

http://www.siam.org/journals/sisc/38-1/M102024.html

†Mathematics Institute, Zeeman Building, University of Warwick, Coventry CV4 7AL, UK (christoph.ortner@warwick.ac.uk). The work of this author was supported by EPSRC grant EP/H003096, ERC Starting Grant 335120, and the Leverhulme Trust through a Philip Leverhulme Prize.

‡Department of Mathematics, Institute of Natural Sciences, and MOE Key Lab in Scientific and Engineering Computing, Shanghai Jiao Tong University, 800 Dongchuan Road, Shanghai 200240, China (lzhang2012@sjtu.edu.cn). The work of this author was supported by NSFC grant 11471214 and 1000 Plan for Young Scientists.

continuum models are blended smoothly. This does not remove, but rather reduces, the error due to ghost forces [26, 10]. The blending variant that we will consider is the blended quasi-continuum (BQCE) scheme, formulated in [26, 14] and analyzed in [26, 10]. These analyses demonstrate that although the error due to ghost forces is reduced, it still remains the dominant error contribution, i.e., the *bottleneck*. Moreover, if the BQCE scheme is generalized to multilattices in the natural way, then the reduced symmetries imply that the scheme would not be convergent in the energy-norm (in the sense of [10]); see the discussions in section 4.3.2 for more details.

In the present paper, we show how a variant of the ghost force correction idea can be used to improve on the BQCE scheme and result in an a/c coupling that we denote blended ghost force correction (BGFC), which is quasi-optimal within the context of the framework developed in [10]. Importantly, within the context in which we present this scheme, our formulation does *not* yield the force-based BQCF scheme [12, 10, 9] but is *energy-based*. As a matter of fact, it is most instructive to construct the scheme not from the point of view of ghost force correction, but through a modification of the site energies.

The remainder of the paper is structured as follows. In section 2 we formulate the BGFC scheme for point defects. In section 3 we extend the benchmark tests from [14, 9, 23] to the new scheme. In section 4 we describe extensions to higher-order finite element, dislocations, and multilattices. Finally, in section 5 we present a rigorous error analysis for the simple-lattice point defect case.

2. The BGFC scheme. For the sake of simplicity of presentation we first present the BGFC scheme in an infinite lattice setting and for point defects. This also allows us to focus on the benchmark problems discussed in [9, 14, 23], which are the main motivation for the introduction of our new scheme. We present extensions to other problems in section 4.

We keep this section relatively formal, but present rigorous formulations and rigorous convergence results in section 5.

2.1. Atomistic model. Consider a *homogeneous reference lattice* $\Lambda^{\rm hom} := \mathsf{A}\mathbb{Z}^d$, $d \in \{2,3\}$, $\mathsf{A} \in \mathbb{R}^{d\times d}$, nonsingular. Let $\Lambda \subset \mathbb{R}^d$ be the *reference configuration*, satisfying $\Lambda \setminus B_{R^{\rm def}} = \Lambda^{\rm hom} \setminus B_{R^{\rm def}}$ and $\#(\Lambda \cap B_{R^{\rm def}}) < \infty$, for some radius $R^{\rm def} > 0$. Here and throughout, $B_R := \{x \in \mathbb{R}^d \,|\, |x| \le R\}$.

The mismatch between Λ and $\Lambda^{\rm hom}$ in $B_{R^{\rm def}}$ represents a possible defect. For example, $\Lambda = \Lambda^{\rm hom}$ for an impurity, $\Lambda \subsetneq \Lambda^{\rm hom}$ for a vacancy, and $\Lambda \supsetneq \Lambda^{\rm hom}$ for an interstitial.

For $a \in \Lambda$, let $\mathcal{N}_a \subset \Lambda \setminus \{a\}$ be a set of "nearest-neighbor" directions satisfying $\mathrm{span}(\mathcal{N}_a) = \mathbb{R}^d$ and $\sup_{a\in\Lambda} \#\mathcal{N}_a < \infty$.

A *deformed configuration* is a map $y : \Lambda \to \mathbb{R}^d$. If it is clear from the context what we mean, then we denote $r_{ab} := |y(a) - y(b)|$ for $a, b \in \Lambda$. We denote the identity map by x.

For each $a \in \Lambda$ let $\Phi_a(y)$ denote the *site energy* associated with the lattice site $a \in \Lambda$. For example, in the EAM (embedded-atom method) model [2],

$$\Phi_a(y) := \sum_{b\in\Lambda\setminus\{a\}} \phi(r_{ab}) + G\Big(\textstyle\sum_{b\in\Lambda\setminus\{a\}} \rho(r_{ab})\Big) \tag{2.1}$$

for a pair potential ϕ, an electron density function ρ, and an embedding function G. We assume that the potentials have a finite interaction range, that is, there exists $r_{\rm cut} > 0$ such that $\partial^j_{y(b)} \Phi_a(y) = 0$ for all $j \ge 1$, whenever $r_{ab} > r_{\rm cut}$, and that they

are homogeneous outside the defect region $B_{R^{\rm def}}$. The latter assumption is discussed in detail in section 2.2.

To describe, e.g., impurity defects, we allow ϕ, G, ρ to be species dependent, i.e., $\phi = \phi_{ab}, G = G_a, \rho = \rho_{ab}$.

Under suitable conditions on the site potentials $\Phi_a, a \in \Lambda$ (most crucially, regularity and homogeneity outside the defect; cf. section 2.2), it is shown in [8] that the energy-difference functional

$$\mathscr{E}^{\rm a}(u) := \sum_{a\in\Lambda} \Phi_a'(u), \quad \text{where } \Phi_a'(u) := \Phi_a(x+u) - \Phi_a(x), \tag{2.2}$$

is well-defined for all relative *displacements* $u \in \mathscr{U}$, where $\mathscr{U}$ is given by

$$\mathscr{U} := \big\{ v : \Lambda \to \mathbb{R}^d \,\big|\, |v|_{\mathscr{U}} < +\infty \big\}, \quad \text{where}$$
$$|v|_{\mathscr{U}} := \left(\sum_{a\in\Lambda} \sum_{b\in\mathcal{N}_a} |v(b) - v(a)|^2 \right)^{1/2}.$$

The atomistic problem is to compute

$$u^{\rm a} \in \arg\min \big\{ \mathscr{E}^{\rm a}(v) \,\big|\, v \in \mathscr{U} \big\}. \tag{2.3}$$

This problem is analyzed in considerable detail in [8].

2.2. Homogeneous crystals. We briefly discuss homogeneity of site potentials, a concept which is important for the introduction of the BGFC scheme and which also plays a crucial role in the analysis of the atomistic model (2.3) in [8].

Homogeneity of the site potential outside the defect core entails simply that only one atomic species occurs. For finite-range interactions, this can be formalized by requiring that, for $|a|, |b|$ sufficiently large, $\Phi_a(y) = \Phi_b(z)$ where $z(\ell) = y(\ell + a - b)$ within the interaction range of b, and suitably extended outside.

For the case $\Lambda = \Lambda^{\rm hom}$ we say that the site potentials are *globally homogeneous* if $\Phi_a(y) = \Phi_b(z)$ for all $a, b \in \Lambda^{\rm hom}$. In this case, it is easy to see (with either summation by parts or point symmetry of the lattice) that

$$\sum_{a\in\Lambda^{\rm hom}} \big\langle \delta\Phi_a(x), u \big\rangle = 0 \quad \forall u : \Lambda^{\rm hom} \to \mathbb{R}^d, \text{supp}(u) \text{ compact}.$$

For general Λ, suppose that the site potentials are homogeneous outside $B_{R^{\rm def}}$, with finite interaction range. Let $\Phi_a^{\rm hom}$, $a \in \Lambda^{\rm hom}$, be a globally homogeneous site potential so that $\langle \delta\Phi_a(x), u\rangle = \langle \delta\Phi_a^{\rm hom}, u\rangle$ for all $a \in \Lambda$, $|a| > R^{\rm def} + r_{\rm cut}$, and for all $u : \Lambda \cup \Lambda^{\rm hom} \to \mathbb{R}^d$ with compact support. Further, for $u : \Lambda \to \mathbb{R}^d$ let Eu denote an arbitrary extension to $\Lambda^{\rm hom}$ (e.g., $Eu(\ell) = 0$ for $\ell \in \Lambda^{\rm hom} \setminus \Lambda$), and let $\Lambda_{\rm def} := \Lambda \cap B_{R^{\rm def}+r_{\rm cut}}$; then

$$\begin{aligned} \mathscr{E}^{\rm a}(u) &= \sum_{a\in\Lambda} \Phi_a'(u) - \sum_{a\in\Lambda^{\rm hom}} \langle \delta\Phi_a^{\rm hom}(x), Eu\rangle \\ &= \sum_{a\in\Lambda} \Phi_a''(u) + \langle L^{\rm ren}, u\rangle, \end{aligned} \tag{2.4}$$

where

$$\Phi_a''(u) := \Phi_a(x+u) - \Phi_a(x) - \langle \delta\Phi_a(x), Eu\rangle, \tag{2.5}$$

$$\langle L^{\rm ren}, u\rangle := \sum_{a\in\Lambda_{\rm def}} \langle \delta\Phi_a(x), u\rangle - \sum_{a\in\Lambda_{\rm def}^{\rm hom}} \langle \delta\Phi_a^{\rm hom}(x), Eu\rangle \tag{2.6}$$

and where $\Lambda_{\rm def}^{\rm hom} := \Lambda^{\rm hom} \cap B_{R^{\rm def}+r_{\rm cut}}$.

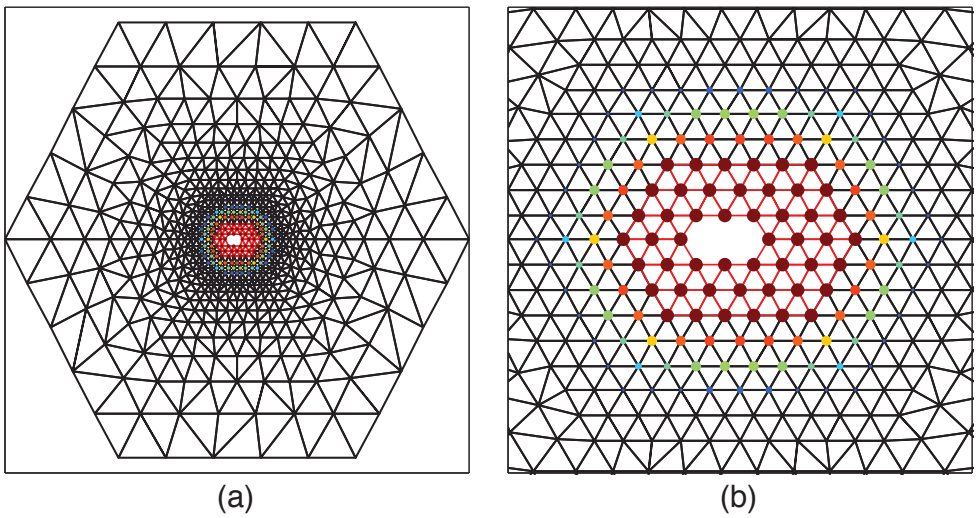

FIG. 1. *Computational domain, finite element grid, and atomistic region as used in the construction of the BQCE and BGFC schemes. The size and color of the spheres in* (b) *indicate the value of the blending function (large/red stands for* $\beta = 0$*).*

The "renormalization" (2.4) of $\mathscr{E}^{\rm a}$ is the basis for proving that $\mathscr{E}^{\rm a}$ is well-defined on the energy space $\mathscr{U}$ [8].

2.3. Continuum model. Suppose that the site potentials are homogeneous outside the defect core, and let $\Phi_a^{\rm hom}$ be the associated globally homogeneous site potentials for the homogeneous lattice; cf. section 2.2.

To formulate atomistic-to-continuum coupling schemes we require a continuum model compatible with (2.2) defined through a strain energy function $W : \mathbb{R}^{d\times d} \to \mathbb{R}$. A typical choice in the multiscale context is the Cauchy–Born model, which is defined via

$$W(\mathsf{F}) := \det \mathsf{A}^{-1} \Phi_0^{\rm hom}(\mathsf{F}x),$$

which represents the energy per unit volume in the homogeneous crystal $\mathsf{F}\Lambda^{\rm hom} = \mathsf{FA}\mathbb{Z}^d$. The associated strain energy difference is denoted by $W'(\mathsf{G}) := W(\mathsf{I}+\mathsf{G}) - W(\mathsf{I})$.

2.4. Standard blending scheme. To formulate the BQCE scheme as introduced in [26, 14] and analyzed in [10] we begin by defining a regular simplicial finite element grid $\mathcal{T}_h$ with nodes $\mathcal{X}_h$, with the minimal requirement that $\mathcal{X}_h \cap B_{R^{\rm def}} = \Lambda \cap B_{R^{\rm def}}$ (that is, the defect core is resolved exactly). Let DOF $:= \#\mathcal{X}_h$. Let $\Omega_h := \bigcup \mathcal{T}_h \supset B_{R^{\rm c}}$, with $R^{\rm c} \geq R^{\rm def}$ the resulting computational domain, and let the space of coarse-grained admissible displacements be given by

$$\mathscr{U}_h := \big\{ v_h \in C(\mathbb{R}^d; \mathbb{R}^d) \,\big|\, v_h \text{ is piecewise affine with respect to } \mathcal{T}_h, \text{ and } v_h|_{\mathbb{R}^d \setminus \Omega_h} = 0 \big\}.$$

Let Q_h denote the P0 midpoint interpolation operator, so that $\int_{\Omega_h} Q_h f$ is the midpoint rule approximation to $\int_{\Omega_h} f$.

Further, let $\beta \in C^{2,1}(\mathbb{R}^d)$ with $\beta = 0$ in $B_{R^{\rm a}}$ with $R^{\rm def} \leq R^{\rm a} < R^{\rm c}$ and $\beta = 1$ in $\mathbb{R}^d \setminus \Omega_h$; then we define the BQCE energy functional (see Figure 1)

$$\mathscr{E}^{\rm b}(u_h) := \sum_{a\in\Lambda\cap\Omega_h} (1-\beta(a))\Phi_a'(u) + \int_{\Omega_h} Q_h\big[\beta W'(\nabla u_h)\big].$$

The BQCE problem is to compute

$$u_h^{\rm b} \in \arg\min \left\{ \mathscr{E}^{\rm b}(v_h) \,\middle|\, v_h \in \mathscr{U}_h \right\}. \tag{2.7}$$

2.5. Review of error estimates. We present a formal review of error estimates for the BQCE scheme established in [14, 10]. This discussion will motivate our construction of the BGFC scheme in the next section.

Under a range of technical assumptions on $\mathcal{T}_h$ and β, it is shown in [10] that if $u^{\rm a}$ is a strongly stable (positivity of the hessian) solution to (2.3), and $(\beta, \mathcal{T}_h)$ are "sufficiently well-adapted to $u^{\rm a}$," then there exists a solution $u_h^{\rm b}$ to (2.7) such that

$$\|\nabla u_h^{\rm b} - \nabla \bar{u}^{\rm a}\|_{L^2} \leq C_1 \|\nabla^2 \beta\|_{L^2} + C_2 \Big(\|\beta h \nabla^2 \tilde{u}^{\rm a}\|_{L^2(\Omega_h)} + \|\nabla \tilde{u}^{\rm a}\|_{L^2(\mathbb{R}^d \setminus B_{R^{\rm c}/2})} \Big) + \dots, \tag{2.8}$$

where "..." denotes formally higher-order terms, $\bar{u}^{\rm a}$ denotes a P1 interpolant on the atomistic grid Λ, and $\tilde{u}^{\rm a}$ denotes a $C^{2,1}$-conforming interpolant on the atomistic grid Λ (intuitively, $\nabla^j \tilde{u}^{\rm a}$, $j \geq 2$, measure the local regularity of $u^{\rm a}$; see section 5 and [10] for more details). The constants depend on (derivatives of) $\Phi_a, a \in \Lambda$, in a way that we will discuss in more detail below.

The term $\|\beta h \nabla^2 \tilde{u}^{\rm a}\|_{L^2(\Omega_h)}$ measures the finite element approximation error, while the term $\|\nabla \tilde{u}^{\rm a}\|_{L^2(\mathbb{R}^d \setminus B_{R^{\rm c}/2})}$ measures the error committed by truncating to a finite computational domain. Exploiting the generic decay rates [8]

$$\begin{aligned} |\nabla^j \tilde{u}^{\rm a}(x)| &\lesssim |x|^{1-d-j} \quad \text{for } j = 0, \dots, 3 \text{ and} \\ |\nabla^j \bar{u}^{\rm a}(x)| &\lesssim |x|^{1-d-j} \quad \text{for } j = 0, 1, \end{aligned} \tag{2.9}$$

these terms can be balanced by ensuring that $R^{\rm c} \approx (R^{\rm a})^{d/2+1}$ and that the mesh is coarsened according to $h(x) \approx (|x|/R^{\rm a})^{3/2}$ (see [21] for the two-dimensional (2D) case; the three-dimensional (3D) case is an immediate extension), which yields

$$\|\beta h \nabla^2 \tilde{u}^{\rm a}\|_{L^2(\Omega_h)} + \|\nabla \tilde{u}^{\rm a}\|_{L^2(\mathbb{R}^d \setminus B_{R^{\rm c}/2})} \lesssim ({\rm DOF})^{-1/2-1/d}.$$

By contrast, the term $\|\nabla^2 \beta\|_{L^2}$ is due to the (smeared) ghost forces, and even an optimal choice of β (balanced against the atomistic region radius $R^{\rm a}$) yields only

$$\|\nabla^2 \beta\|_{L^2} \approx ({\rm DOF})^{1/2-2/d}. \tag{2.10}$$

To see this we note that a quasi-optimal choice is $\beta(x) = B(r)$, where B is a radial spline with $B(r) = 0$ for $r \leq R^{\rm a}$ and $B(r) = 1$ for $r \geq R^{\rm b} \in (R^{\rm a}, R^{\rm c})$ (see [26, 14] for in-depth discussions). A straightforward computation (assuming $R^{\rm b} \lesssim R^{\rm a}$; the case $R^{\rm b} \gg R^{\rm a}$ is similar) then shows that $\|\nabla^2 \beta\|_{L^2}^2 \approx (R^{\rm b})^{d-1}(R^{\rm b} - R^{\rm a})^{-3} + (R^{\rm b} - R^{\rm a})^{d-4}$, which is optimized subject to fixing the total number of degrees of freedom (DOF) if $R^{\rm b} - R^{\rm a} \approx R^{\rm a}$. This yields precisely (2.10).

In summary, for this simple model problem, the BQCE scheme's rate of convergence,

$$\|\nabla u_h^{\rm b} - \nabla \bar{u}^{\rm a}\|_{L^2} \lesssim ({\rm DOF})^{1/2-2/d},$$

is the same in two dimensions and worse in three dimensions than a straightforward truncation scheme, in which the atomistic model is minimized over a finite computational domain (see [8]). Analogous results hold also for dislocations.

2.6. The BGFC scheme. The motivation for the BGFC scheme is to optimize the coefficient C_1 in (2.8). An investigation of the analysis in sections 6.1 and 6.2 in [10] reveals that a simple upper bound is

$$C_1 \lesssim \sup_{a\in\Lambda\cap\mathrm{supp}(\beta)} \sup_{b\in\Lambda\setminus\{a\}} \Big| \frac{\partial \Phi_a(y)}{\partial y(b)}|_{y=x+u} \Big|.$$

(As a matter of fact, this form of C_1 requires a minor modification of the remaining error estimates [10]; however, we use it only for motivation.)

The idea is to "renormalize" the interatomic potential so that $\delta\Phi_a(x) = 0$ for $|a|$ sufficiently large, which would then ensure that $|\partial_{y(b)}\Phi_a(x+u)| \lesssim |u(b)-u(a)|$, and hence would yield additional decay of the constant C_1 as the atomistic region increases.

Recalling the discussion in section 2.2 we note that $\delta\Phi_a''(x) = 0$ for all $a \in \Lambda$. Thus, if we apply the blending procedure to the renormalized atomistic energy (2.4), then we would obtain a new constant C_1'', with

$$\begin{aligned} C_1'' &\lesssim \sup_{a\in\Lambda\cap\mathrm{supp}(\nabla\beta)} \sup_{\substack{b\in\Lambda\setminus\{a\}\\ r_{ab}\le r_{\mathrm{cut}}}} \big|\partial_{y(b)}\Phi_a''(x+u)\big| \\ &= \sup_{a\in\Lambda\cap\mathrm{supp}(\nabla\beta)} \sup_{\substack{b\in\Lambda\setminus\{a\}\\ r_{ab}\le r_{\mathrm{cut}}}} \big|\partial_{y(b)}\Phi_a(x+u) - \partial_{y(b)}\Phi_a(x)\big| \\ &\lesssim C_2 \big\|\nabla \bar{u}^{\mathrm{a}}\big\|_{L^\infty(\mathbb{R}^d\setminus B_{R^{\mathrm{a}}-2r_{\mathrm{cut}}})} \lesssim (R^{\mathrm{a}})^{-d}, \end{aligned}$$

where the second-to-last inequality is true for sufficiently large R^{a} and the last inequality follows from the decay estimate given in [8, Thm. 3.1]. We therefore obtain

$$C_1''\|\nabla^2\beta\|_{L^2} \lesssim (\mathrm{DOF})^{-1/2-2/d}, \tag{2.11}$$

which not only balances the best approximation error but is even dominated by it.

To summarize, the BGFC energy (difference) functional reads

$$\mathscr{E}^{\mathrm{bg}}(u_h) := \sum_{a\in\Lambda\cap\Omega_h} (1-\beta(a))\Phi_a''(u_h) + \int_{\Omega_h} Q_h\big[\beta W''(\nabla u_h)\big] + \langle L^{\mathrm{ren}}, u_h\rangle, \tag{2.12}$$

where Φ_a'' is defined in (2.5), L^{ren} is defined in (2.6), and $W''(\mathsf{F}) := W(\mathsf{I}+\mathsf{F}) - W(\mathsf{I}) - \partial W(\mathsf{I}) : \mathsf{F}$. The associated variational problem is

$$u_h^{\mathrm{bg}} \in \arg\min\big\{\mathscr{E}^{\mathrm{bg}}(v_h) \,\big|\, v_h \in \mathscr{U}_h\big\}. \tag{2.13}$$

We can further optimize the BGFC scheme as follows. If $R^{\mathrm{b}}/R^{\mathrm{a}} \sim c$ as $R^{\mathrm{a}} \to \infty$, then the coupling error of the BGFC scheme scales like $(R^{\mathrm{a}})^{-d/2-2}$, and is therefore dominated by the best approximation error, which scales like $(R^{\mathrm{a}})^{-d/2-1}$. To reduce computational cost (by a constant factor), we can balance these two terms. Making the ansatz $R^{\mathrm{b}} - R^{\mathrm{a}} \sim (R^{\mathrm{a}})^t$ for $t \in (0,1)$, and noting that we can always construct β such that $|\nabla^2\beta| \lesssim (R^{\mathrm{a}})^{-t}$, we obtain that

$$C_1''\|\nabla^2\beta\|_{L^2} \lesssim (R^{\mathrm{a}})^{-d/2-3/2-1/2}.$$

This is balanced with the best approximation rate, $(R^{\mathrm{a}})^{-d/2-1}$, if $t = 1/3$.

We therefore conclude that if $R^{\mathrm{b}} - R^{\mathrm{a}} \approx (R^{\mathrm{a}})^t$ for some $t \ge 1/3$, then we expect the BGFC scheme to obey the error estimate

$$\|\nabla u_h^{\mathrm{bg}} - \nabla \bar{u}^{\mathrm{a}}\|_{L^2} \lesssim (R^{\mathrm{a}})^{-d/2-1} \approx (\mathrm{DOF})^{-1/2-1/d}.$$

We shall make this rigorous for a slightly simplified formulation in section 5, where we will also prove an energy error estimate.

2.7. Connection to ghost force correction and generalization. Consider, for simplicity, the case when $\Phi_a^{\rm hom} \equiv \Phi_a$, i.e., the crystal is homogeneous. In this case, $L^{\rm ren} \equiv 0$ as well. Moreover, we can rewrite the BGFC scheme as follows:

$$\begin{aligned}\mathscr{E}^{\rm bg}(u_h) &= \mathscr{E}^{\rm b}(u_h) - \sum_{a\in\Lambda}(1-\beta(a))\langle \delta\Phi_a(0), u_h\rangle - \int_{\mathbb{R}^d} Q_h\big[\beta\partial W(0) : \nabla u_h\big]\,{\rm d}x \\ &= \mathscr{E}^{\rm b}(u_h) - \langle \delta\mathscr{E}^{\rm b}(0), u_h\rangle \\ &= \mathscr{E}^{\rm b}(u_h) - \langle \delta\mathscr{E}^{\rm b}(0) - \mathcal{F}^{\rm bqcf}(0), u_h\rangle, \qquad (2.14)\end{aligned}$$

where $\mathcal{F}^{\rm bqcf}$ is the BQCF operator defined in [9], and $\mathcal{F}^{\rm bqcf}(0) = 0$ (this nonconservative a/c coupling has no ghost forces). Thus, we see that the renormalization step $\Phi_a' \rightsquigarrow \Phi_a''$ (cf. (2.2) and (2.5)) is equivalent to the dead load ghost force correction scheme of Shenoy at al. [24], applied for a blended coupling formulation and in the reference configuration.

This immediately suggests the following generalization of the BGFC scheme:

$$\mathscr{E}^{\rm bg}(u_h) := \mathscr{E}^{\rm b}(u_h) - \big\langle \delta\mathscr{E}^{\rm b}(\hat{u}_h) - \mathcal{F}^{\rm bqcf}(\hat{u}_h), u_h - \hat{u}_h\big\rangle, \qquad (2.15)$$

where $\hat{u}_h$ is a suitable reference configuration, or "predictor," that can be cheaply obtained.

We will explore this alternative point of view in future work, in particular with an eye to applications involving cracks and edge dislocations. Note that this generalization cannot be written within the renormalization formulations.

3. Numerical tests.

3.1. Model problems. Our prototype implementation of BGFC is for the 2D triangular lattice $\mathsf{A}\mathbb{Z}^2$ defined by

$$\mathsf{A} = \begin{pmatrix} 1 & \cos(\pi/3) \\ 0 & \sin(\pi/3)\end{pmatrix}.$$

To generate a defect, we remove k atoms

$$\begin{cases} \Lambda_k^{\rm def} := \big\{-(k/2+1)e_1, \dots, k/2 e_1\big\} & \text{if } k \text{ is even,} \\ \Lambda_k^{\rm def} := \big\{-(k-1)/2 e_1, \dots, (k-1)/2 e_1\big\} & \text{if } k \text{ is odd,}\end{cases}$$

to obtain $\Lambda := \mathsf{A}\mathbb{Z}^2 \setminus \Lambda_k^{\rm def}$. For small k, the defect acts like a point defect, while for large k it acts like a small crack embedded in the crystal. In our experiments we shall consider $k = 2$ (di-vacancy) and $k = 11$ (microcrack), following [14, 9, 23].

The site energy is given by an EAM (toy) model (3.1) [2], for which Φ_ℓ is of the form

$$\begin{aligned}\Phi_\ell(y) &= \sum_{\rho\in\mathcal{R}(\ell)} \phi\big(|D_\rho y(\ell)|\big) + F\Big(\textstyle\sum_{\rho\in\mathcal{R}(\ell)}\psi\big(|D_\rho y(\ell)|\big)\Big), \qquad (3.1)\\ \text{with} \quad & \phi(r) = [e^{-2a(r-1)} - 2e^{-a(r-1)}], \quad \psi(r) = e^{-br}, \\ & F(\tilde{\rho}) = c\big[(\tilde{\rho}-\tilde{\rho}_0)^2 + (\tilde{\rho}-\tilde{\rho}_0)^4\big],\end{aligned}$$

with parameters $a = 4.4, b = 3, c = 5, \tilde{\rho}_0 = 6e^{-b}$. The interaction range is $\mathcal{R}(\ell) = \Lambda \cap B_2(\ell)$, i.e., next nearest neighbors in hopping distance.

To construct the BQCE and BGFC schemes, we choose an elongated hexagonal domain Ω^{a} containing K layers of atoms surrounding the vacancy sites, and the full computational domain Ω_h to be an elongated hexagon containing R^{c} layers of atoms surrounding the vacancy sites. The domain parameters are chosen so that $R^{\mathrm{c}} = \lceil \frac{1}{2}(R^{\mathrm{a}})^2 \rceil$. The finite element mesh is graded so that the mesh size function $h(x) = \mathrm{diam}(T)$ for $T \in \mathscr{T}$ satisfies $h(x) \approx (|x|/R^{\mathrm{a}})^{3/2}$. These choices balance the coupling error at the interface, the finite element interpolation error, and the far-field truncation error [8, sect. 5.2]. Recall, moreover, that DOF $:= \#\mathcal{X}_h$.

The blending function is obtained in a preprocessing step by approximately minimizing $\|\nabla^2 \beta\|_{L^2}$, as described in detail in [14].

We implement the equivalent ghost force removal formulation (2.14) instead of the "renormalization formulation" (2.12).

3.1.1. Di-vacancy. In the di-vacancy test two neighboring sites are removed, i.e., $k = 2$. We apply 3% isotropic stretch and 3% shear loading by setting

$$\mathsf{B} := \begin{pmatrix} 1+s & \gamma_{\mathrm{II}} \\ 0 & 1+s \end{pmatrix} \cdot \mathsf{F}_0,$$

where $\mathsf{F}_0 \propto I$ minimizes W, $s = \gamma_{\mathrm{II}} = 0.03$.

3.1.2. Microcrack. In the microcrack experiment, we remove a longer segment of atoms, $\Lambda_{11}^{\mathrm{def}} = \{-5e_1, \ldots, 5e_1\}$, from the computational domain. The body is then loaded in mixed modes I and II by setting

$$\mathsf{B} := \begin{pmatrix} 1 & \gamma_{\mathrm{II}} \\ 0 & 1+\gamma_{\mathrm{I}} \end{pmatrix} \cdot \mathsf{F}_0,$$

where $\mathsf{F}_0 \propto I$ minimizes W, and $\gamma_{\mathrm{I}} = \gamma_{\mathrm{II}} = 0.03$ (3% shear and 3% tensile stretch).

3.2. Methods. We test the BGFC method with blending widths $K := R^{\mathrm{b}} - R^{\mathrm{a}} = \lceil (R^{\mathrm{a}})^{1/3} \rceil$ and with $K = R^{\mathrm{b}} - R^{\mathrm{a}} = R^{\mathrm{a}}$ (here, the blending width denotes the number of hexagonal atomic layers in the blending region). The BGFC scheme is compared against the following three competitors previously considered in [14, 9, 23]:

- BQCE: blended quasi-continuum method, implementation based on [14], with most details described in section 2.4.
- GRAC: sharp-interface consistent energy-based a/c coupling [23].
- BQCF: blended force-based a/c coupling, as described in [9]. Energies of BQCF are computed using BQCE (i.e., the BQCE energy is evaluated at the BQCF solution).

3.3. Results. We present two experiments, a di-vacancy ($k = 2$) and a microcrack ($k = 11$). For each test, we choose an increasing sequence of atomistic region sizes R^{a}, followed by the quasi-optimal choices of $R^{\mathrm{b}}, \Omega_h, \beta$ as described above.

For both experiments we plot the absolute errors against the number of DOF, which is proportional to computational cost, in the H^1-seminorm, the $W^{1,\infty}$-seminorm, and the (relative) energy.

The results are shown in Figures 2, 3, and 4 for the di-vacancy problem and in Figures 5, 6, and 7 for the microcrack problem.

In the first experiment, we are able to clearly observe the predicted asymptotic behavior of the a/c coupling schemes, while in the second experiment we observe a significant preasymptotic regime, where the analytic predictions become relevant only at fairly high resolutions.

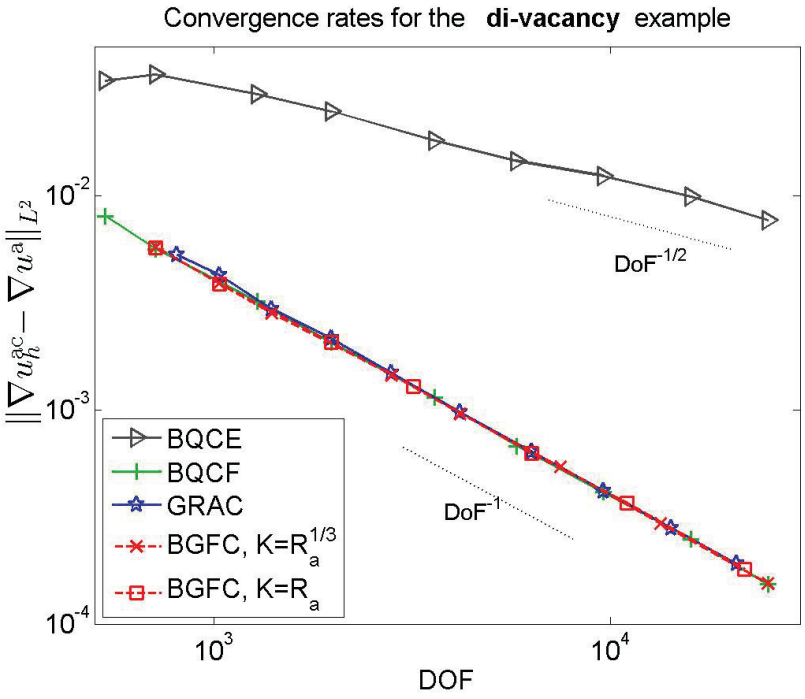

FIG. 2. *Convergence rates in the energy-norm (the H^1-seminorm) for the di-vacancy benchmark problem described in section* 3.1.1.

In all error graphs, we clearly observe the optimal convergence rate of BGFC, together with the other consistent methods GRAC and BQCF, while BQCE has a suboptimal rate. Recall, however, that the BGFC scheme comes with the following added advantages: over GRAC it is straightforward to construct, and over BQCF it is energy-based.

4. Extensions. It is possible to extend the formulation of the BGFC scheme to a much wider range of problems, including, e.g., multiple defect regions, problems with surfaces (e.g., nano-indentation, crack propagation), complex crystals, or higher-order finite elements. We now present a range of such generalizations, arguing again only formally.

4.1. Higher-order finite elements. We have seen in section 2.6 that in the BGFC scheme applied to point defects, the approximation error dominates the blending (coupling) error. This particular bottleneck is relatively straightforward to remove by increasing the order of the finite element scheme and the size of the continuum region. The following discussion is motivated by [3].

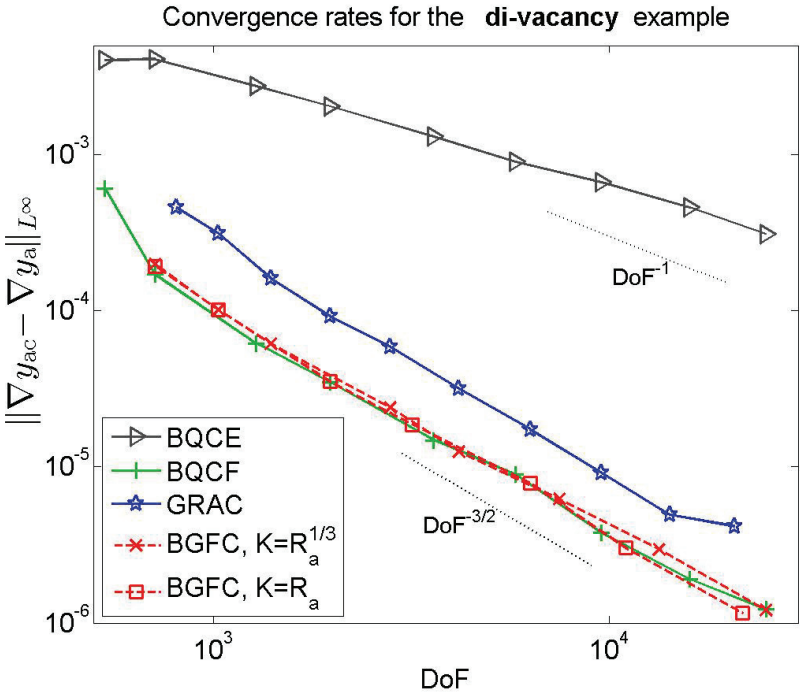

FIG. 3. *Convergence rates in the $W^{1,\infty}$-seminorm for the di-vacancy benchmark problem described in section* 3.1.1.

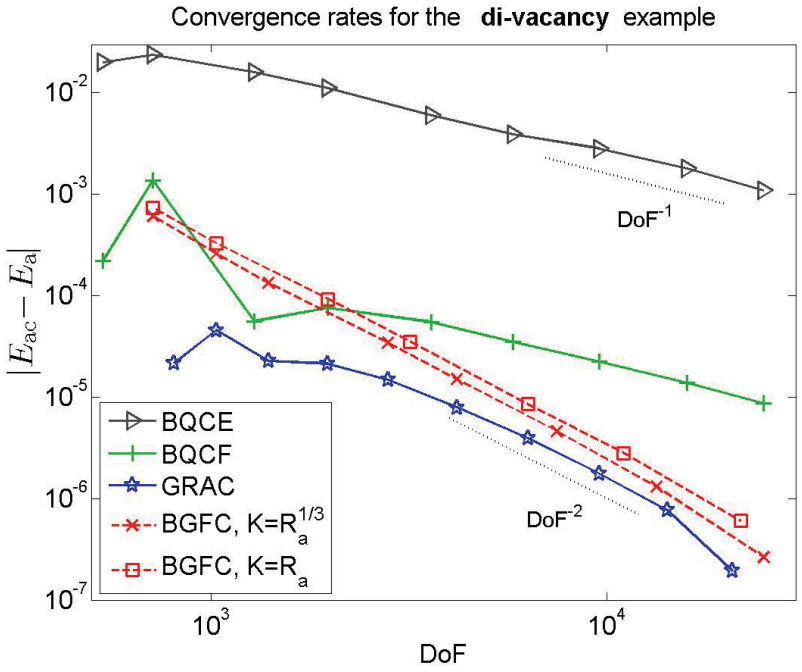

FIG. 4. *Convergence rates in the relative energy for the di-vacancy benchmark problem described in section* 3.1.1.

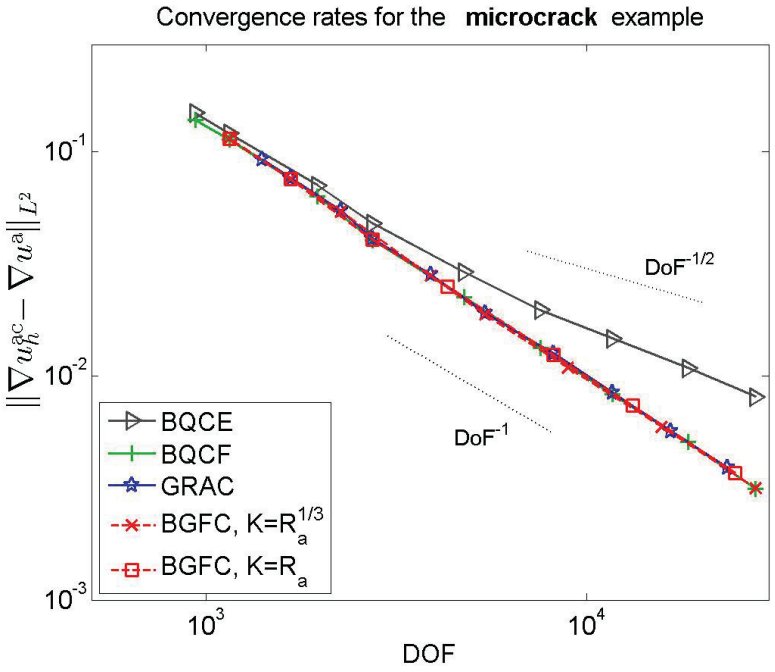

FIG. 5. *Convergence rates in the energy-norm (the H^1-seminorm) for the microcrack benchmark problem with $\Lambda_{11}^{\rm def}$ described in section* 3.1.2.

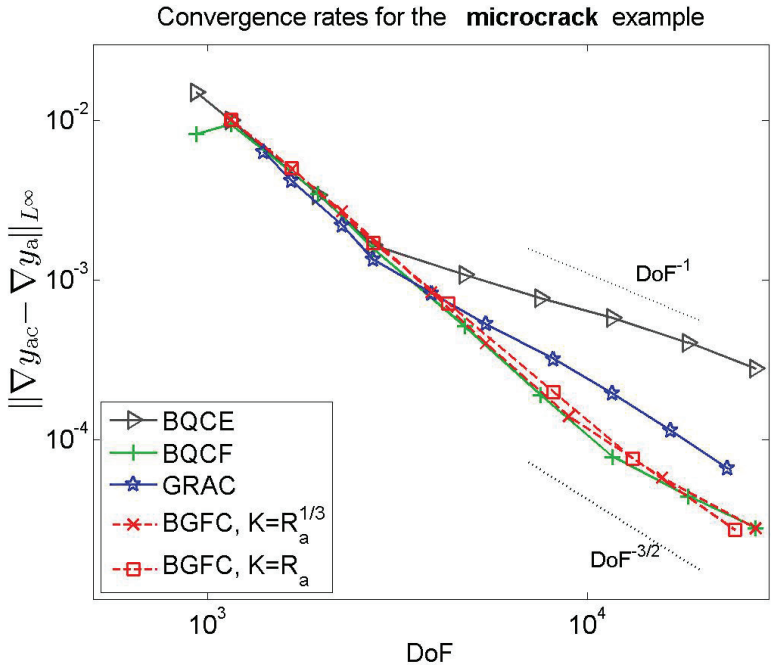

FIG. 6. *Convergence rates in the $W^{1,\infty}$-seminorm for the microcrack benchmark problem with $\Lambda_{11}^{\rm def}$ described in section* 3.1.2.

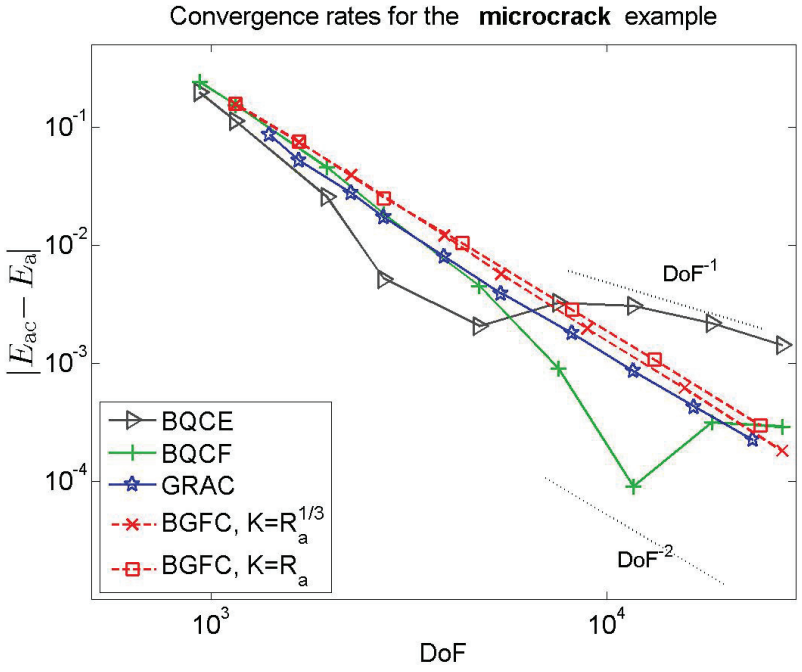

FIG. 7. *Convergence rates in the relative energy for the microcrack benchmark problem with* $\Lambda_{11}^{\mathrm{def}}$ *described in section* 3.1.2.

We construct the computational domain and finite element mesh in the same way as in sections 2.6 and 3. We decompose $\mathcal{T}_h = \mathcal{T}_h^{(\mathrm{P1})} \cup \mathcal{T}_h^{(\mathrm{P2})}$, where

$$\mathcal{T}_h^{(\mathrm{P1})} = \big\{T \in \mathcal{T}_h \,\big|\, \beta|_T < 1\big\},$$

and replace $\mathscr{U}_h$ with the approximation space

$$\begin{aligned}\mathscr{U}_h^{(2)} := \big\{u_h \in C(\mathbb{R}^d;\mathbb{R}^d)\,\big|\;& u_h|_T \text{ is affine for } T \in \mathcal{T}_h^{(\mathrm{P1})},\\ & u_h|_T \text{ is quadratic for } T \in \mathcal{T}_h^{(\mathrm{P2})}, \text{ and}\\ & u_h = 0 \text{ in } \mathbb{R}^d \setminus \Omega_h\big\}.\end{aligned} \tag{4.1}$$

That is, we retain the P1 discretization in the fully refined atomistic and blending region where Λ and $\mathcal{X}_h$ coincide, but employ P2 finite elements in the continuum region. To ensure stability, the quadrature operator Q_h (previously midpoint interpolation) must now be adjusted to provide a third-order quadrature scheme (e.g., the face midpoint trapezoidal rule) so that $\nabla u_h \otimes \nabla u_h$ for $u_h \in \mathscr{U}_h^{(2)}$ can be integrated exactly.

The resulting P2-BGFC method reads

$$u_h \in \arg\min\big\{\mathcal{E}^{\mathrm{bg}}(u_h)\,\big|\,u_h \in \mathscr{U}_h^{(2)}\big\}.$$

4.1.1. Convergence rate. The blending error and the Cauchy–Born modeling error contributions to the P2-BGFC method remain the same as those for the P1-BGFC method, $C_1''\|\nabla^2\beta\|_{L^2} \lesssim (R^{\mathrm{a}})^{-d/2-2}$; see (2.11) in section 2.6. Only the

approximation error component must be reconsidered. It is reasonable to expect (and we make this rigorous in section 6; interestingly, this is a nontrivial generalization) that the best approximation error contribution can be bounded by

$$\|h^2\nabla^3\tilde{u}^{\mathrm{a}}\|_{L^2(\Omega_h\setminus B_{R^{\mathrm{a}}})} + \|\nabla\tilde{u}^{\mathrm{a}}\|_{L^2(\mathbb{R}^d\setminus B_{R^{\mathrm{c}}/2})},$$

where the first term is the standard P2 finite element best approximation error and the second term is the far-field truncation error.

Choosing $h(x) \approx \max(1, (|x|/R^{\mathrm{b}})^{3/2})$ and an increased continuum region $R^{\mathrm{c}} \approx (R^{\mathrm{a}})^{1+4/d}$, a straightforward computation, employing the generic decay rates (2.9) for point defects, shows that the two terms are balanced and bounded by

$$\begin{aligned}\|h^2\nabla^3\tilde{u}^{\mathrm{a}}\|_{L^2(\Omega_h\setminus B_{R^{\mathrm{a}}})}+\|\nabla\tilde{u}^{\mathrm{a}}\|_{L^2(\mathbb{R}^d\setminus B_{R^{\mathrm{c}}/2})} &\lesssim \left(\int_{R^{\mathrm{a}}}^{\infty} r^{d-1}\left(\tfrac{r}{R^{\mathrm{a}}}\right)^3 r^{-2d-4}\,\mathrm{d}r\right)^{1/2} + (R^{\mathrm{c}})^{-d/2}\\ &\lesssim (R^{\mathrm{a}})^{-d/2-2} \approx (\mathrm{DOF})^{-1/2-2/d}.\end{aligned}$$

It is possible to make this construction without violating the necessary mesh regularity required to obtain the stated finite element approximation error; see [16] for further discussion.

Thus we (formally) obtain

$$\|\nabla u_h^{\mathrm{bg}} - \nabla\bar{u}^{\mathrm{a}}\|_{L^2} \lesssim (R^{\mathrm{a}})^{-d/2-2} \approx (\mathrm{DOF})^{-1/2-2/d}.$$

It is particularly interesting to note that the Cauchy–Born modeling error contribution is also bounded by

$$\|\nabla^3\tilde{u}^{\mathrm{a}}\|_{L^2(\Omega_h\setminus B_{R^{\mathrm{a}}})} + \|\nabla^2\tilde{u}^{\mathrm{a}}\|^2_{L^4(\Omega_h\setminus B_{R^{\mathrm{a}}})} \lesssim (R^{\mathrm{a}})^{-d/2-2} \approx (\mathrm{DOF})^{-1/2-2/d},$$

and one may expect that this bound is optimal in most cases. Thus, we see that for the P2-BGFC method, all three error components (coupling error, approximation error, Cauchy–Born modeling error) are balanced in the energy-norm. In particular, this means that, for point defects, the P2-BGFC scheme is *quasi-optimal* among all a/c coupling methods that employ the Cauchy–Born model in the continuum region.

4.1.2. Numerical experiment. We test the P2-BGFC method with blending widths $K := R^{\mathrm{b}} - R^{\mathrm{a}} = R^{\mathrm{a}}$ and $R^{\mathrm{c}} = (R^{\mathrm{a}})^3$. In Figure 8, for the di-vacancy benchmark problem, we show an energy-norm convergence rate of P2-BGFC together with BQCE, BQCF, GRAC, and P1-BGFC with $K := R^{\mathrm{b}} - R^{\mathrm{a}} = \lceil (R^{\mathrm{a}})^{1/3} \rceil$. The predicted rate $(\mathrm{DOF})^{-3/2}$ is justified by the numerical results.

4.2. Screw dislocation. We briefly demonstrate how the BGFC scheme may be formulated for simulating a screw dislocation. The ideas are a straightforward combination of those in [8] and section 2 of the present paper, and thus we only present minimal details.

For the sake of simplicity, we restrict the discussion and implementation to nearest-neighbor interaction and antiplane shear motion, following [8, sect. 6.2]. That is, we define $\Lambda = \Lambda^{\mathrm{hom}} = \mathsf{A}\mathbb{Z}^2$, where

$$\mathsf{A} = \begin{pmatrix} 1 & \cos(\frac{\pi}{3}) \\ 0 & \sin(\frac{\pi}{3}) \end{pmatrix} \quad \text{and} \quad \mathcal{R} = \{\mathsf{Q}_6^j e_1 \,|\, j = 0, \dots, 5\}$$

is the set of interacting lattice directions. (Note that Λ^{hom} is in fact the projection of a bcc crystal along the (111) direction.) Admissible (antiplane) displacements are maps $y : \Lambda \to \mathbb{R}$.

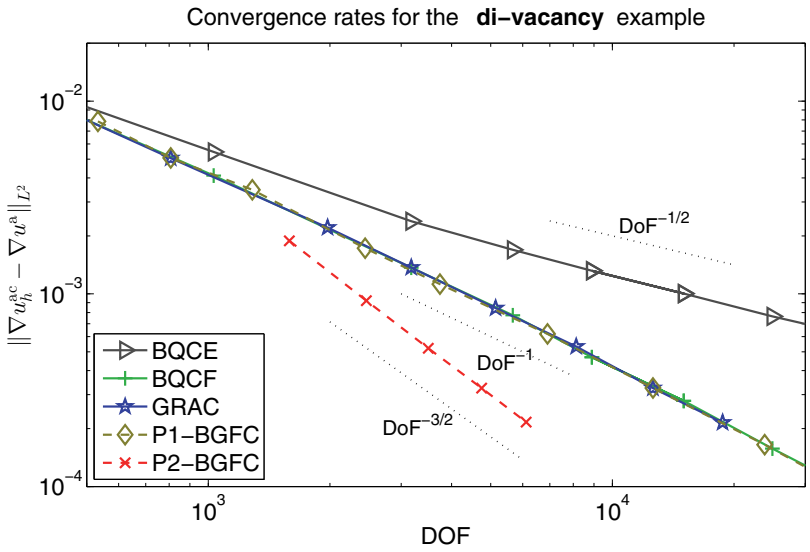

FIG. 8. *Convergence rate of P2-BGFC in the energy-norm (H^1-seminorm) for the di-vacancy benchmark problem described in section* 3.1.1.

The site potential is now a map $\Phi_a \in C^3(\mathbb{R}^6)$, i.e., $\Phi_a(y)$ is a function of $(y(b) - y(a))_{b\in a+\mathcal{R}}$. To admit slip by a Burgers vector (we assume the Burgers vector is $(1,0,0)$), we assume that $\Phi_a(y) = \Phi_a(z)$ whenever $y - z : \Lambda \to \mathbb{Z}$.

A screw dislocation is enforced, e.g., by applying the far-field boundary condition

$$y(a) \sim y^{\rm lin}(a) := \tfrac{1}{2\pi} \arg(a - \hat{a}) \quad \text{as } |a| \to \infty,$$

where $y^{\rm lin}$ is the linearized elasticity solution and $\hat{a}$ is an arbitrary shift of the dislocation core. The model of section 2 can be extended by defining $\Phi'_a(u) := \Phi_a(y^{\rm lin} + u) - \Phi_a(y^{\rm lin})$, and $\mathscr{E}^{\rm a}(u) := \sum_{a\in\Lambda} \Phi'_a(u)$. With this modification the exact model still reads as (2.3); see [8] for details.

To define the BGFC scheme we renormalize Φ_a a second time,

$$\Phi''_a(u) := \Phi_a(y^{\rm lin} + u) - \Phi_a(y^{\rm lin}) - \langle \delta\Phi_a(0), u\rangle,$$

which gives rise to the BGFC functional defined by (2.12). Note that $L^{\rm ren} \equiv 0$ in this case. The resulting BGFC scheme is still given by (2.13).

Remark 1. (1) It is tempting to define

$$\Phi''_a(u) := \Phi_a(y^{\rm lin} + u) - \Phi_a(y^{\rm lin}) - \langle \delta\Phi_a(y^{\rm lin}), u\rangle,$$

which seemingly has advantages in terms of error reduction. However, (i) it has the disadvantage of having to evaluate a nontrivial functional $\langle L^{\rm ren}, u\rangle$, for which a new scheme must be developed; and (ii) the Cauchy–Born modeling error is already dominant in the dislocation case, which means that no further improvements can in fact be expected.

(2) However, taking the alternative view presented in section 2.7, we may (re)define the BGFC scheme as in (2.15), where we note that now the predictor $y^{\rm lin}$ is used for the dead load ghost force removal *without* creating long-ranging residual forces in the continuum region. This may indeed lead to a (moderate) improvement,

which we will analyze in future work, together with applications to edge dislocations, where the "renormalization formulation" seems less straightforward. (We note again that if the "predictor" is not homogeneous, then the GFC and renormalization formulations are no longer equivalent.)

(3) Employing P2 finite elements in the dislocation case does not give higher accuracy, as the rate with P1 elements is already optimal.

4.2.1. Convergence rate. Suppose that the setup of the computational geometry is as in section 2, with the only exception that we now need to take a coarsening rate $h(x) \approx |x|/R^{\rm a}$, due to the quadrature error (see [10]). This only marginally modifies the analysis.

It is shown in [8, Thm. 3.1] under natural technical conditions that if a minimizer $u^{\rm a}$ of the screw dislocation problem exists, then

$$|\nabla^j y_0(x)| \lesssim |x|^{2-j} \quad \text{and} \quad |\nabla^j \tilde{u}^{\rm a}(x)| \lesssim |x|^{-1-j} \log|x|.$$

A QNL-type ghost force free scheme (e.g., geometric-reconstruction–based [23]) is then expected to have an error of the order of magnitude of (see [8, sect. 5.2] for details)

$$\begin{aligned}\|\nabla \bar{u}^{\rm a} - \nabla u_h^{\rm qnl}\|_{L^2} &\lesssim \|h\nabla^2 \tilde{u}^{\rm a}\|_{L^2(\Omega_h \setminus B_{R^{\rm a}})} + \|\nabla \tilde{u}^{\rm a}\|_{L^2(\mathbb{R}^d \setminus B_{R^{\rm c}/2})} \\ &\quad + \|\nabla^2(y_0 + \tilde{u}^{\rm a})\|_{L^2(\Omega^{\rm i})} + \dots \\ &\lesssim (R^{\rm a})^{-2}(\log R^{\rm a})^{1/2} + (R^{\rm a})^{-3/2} \approx (\mathrm{DOF})^{-3/4},\end{aligned}$$

where $u_h^{\rm qnl}$ denotes the solution of such a scheme, $\|\nabla^2(y_0+\tilde{u}^{\rm a})\|_{L^2(\Omega^{\rm i})}$ is the interfacial coupling error (cf. [18]), and we denoted again several dominated terms by "...". We observe that, for QNL-type methods, the coupling error dominates the estimate.

Following the analysis in [10] and sections 2.6 and 5, we can obtain

$$\begin{aligned}\|\nabla \bar{u}^{\rm a} - \nabla u_h^{\rm bg}\|_{L^2} &\lesssim \|\nabla^2 \beta\|_{L^\infty} \|\nabla(y_0 + \tilde{u}^{\rm a})\|_{L^2(\Omega^{\rm b})} + \text{best approx. err.} + \dots \\ &\lesssim (R^{\rm b} - R^{\rm a})^{-2} \big(\log\big(R^{\rm b}/R^{\rm a}\big)\big)^{1/2} + (R^{\rm a})^{-2}(\log R^{\rm a})^{1/2}.\end{aligned}$$

We observe that with $R^{\rm b} - R^{\rm a} \approx (R^{\rm a})^\alpha$ the two errors are balanced for $\alpha = 1$, i.e., $R^{\rm b} - R^{\rm a} \approx R^{\rm a}$, and that in this case we obtain the "optimal rate" (i.e., the best approximation error rate)

$$\|\nabla \bar{u}^{\rm a} - \nabla u_h^{\rm bg}\|_{L^2} \lesssim (R^{\rm a})^{-2}(\log R^{\rm a})^{1/2} \approx (\mathrm{DOF})^{-1}(\log \mathrm{DOF})^{1/2}.$$

Thus, we conclude that the BGFC scheme leads to a better rate of convergence than the QNL-type scheme. This is particularly encouraging as the latter is often assumed optimal among energy-based a/c coupling schemes.

Remark 2. We note that the Cauchy–Born modeling error for the screw dislocation example is bounded, in terms of $y = y_0 + u$, by

$$\|\nabla^3 \tilde{y}\|_{L^2(\Omega_h \setminus B_{R^{\rm a}})} + \|\nabla^2 \tilde{y}\|^2_{L^4(\Omega_h \setminus B_{R^{\rm a}})} \lesssim (R^{\rm a})^{-2} \approx (\mathrm{DOF})^{-1}.$$

Thus, up to logarithmic terms, the best approximation and blending errors are both balanced with the Cauchy–Born modeling error, which is a lower-bound for a/c couplings based on local continuum models. In this sense, the BGFC method is *optimal* for screw dislocations as well.

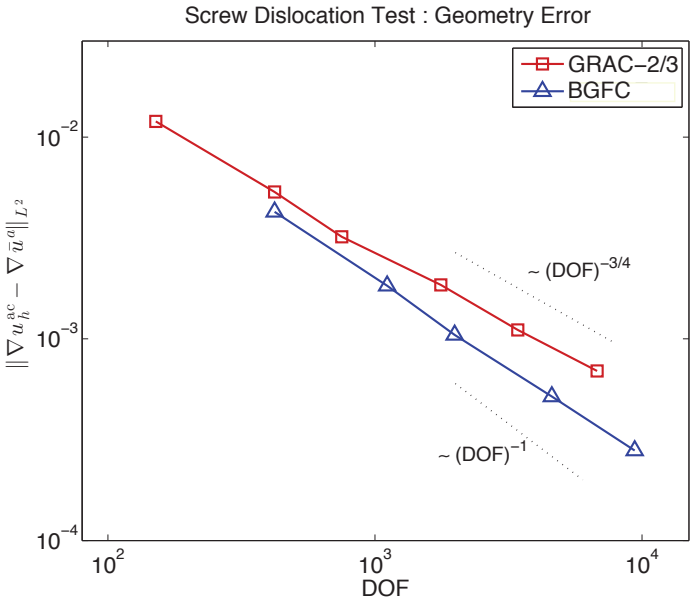

FIG. 9. *Convergence of the QNL-type GRAC-2/3 [22] and of the BGFC schemes for an antiplane screw dislocation problem.*

4.2.2. Numerical experiment. Replicating the setting from [8, sect. 6.2], we use a simplified EAM-type interatomic potential (cf. (2.1)), given by

$$\Phi_a(y) := G\Bigg(\sum_{b\in a+\mathcal{R}} \phi(y(b)-y(a))\Bigg), \quad \text{where} \quad G(s) = 1+\tfrac{1}{2}s^2, \quad \text{and} \quad \phi(r) = \sin^2\big(\pi r\big).$$

Note that, in this case, the BQCE and BGFC methods are in fact identical since $\delta\Phi_a(0) = 0$. (This is an artefact of the antiplane setting.)

We employ the same constructions of the computational domain as in the point defect case described in section 3, but without vacancy sites.

In Figure 9 we compare the GRAC-2/3 method (cf. [22]) with the BGFC scheme. We observe numerical rates that are close to the predicted ones, and in particular also the moderate improvement of BGFC over GRAC-2/3 suggested in the previous section.

4.3. Complex crystals. To formulate the BGFC scheme for complex crystals, we return to the point defect problem addressed in section 2.

4.3.1. Atomistic model. Each lattice site may now contain more than one atom (of the same or different species). For simplicity suppose there are two atoms per site, which we call species 1 and species 2. The deformation of the lattice is now described by a deformation field $y : \Lambda \to \mathbb{R}^d$ and a shift $p : \Lambda \to \mathbb{R}^d$. The deformed positions of species 1 are given by $y_1(a) := y(a)$, and those of species 2 by $y_2(a) := y(a) + p(a)$, $a \in \Lambda$. Let $\mathbf{y} := (y, p)$. The site energy is now a function

$$\Phi_a(\mathbf{y}) = \Phi_a\Bigg(\big(y_i(b)-y_j(a)\big)_{\substack{i,j=1,2\\ b\in\Lambda}}\Bigg).$$

At present there exists no published regularity theory for complex lattice defects corresponding to [8], which we employed in the discussion in section 2, and the following discussion is therefore based on unpublished notes [19, 17] and reasonable assumptions.

Let $\Phi_a^{\rm hom}$ be the site energy potential for the defect-free lattice; then we assume that there is an equilibrium shift p_0 such that $\mathbf{x} := (x, p_0)$ is a stable equilibrium configuration. By this, we mean that for all $\mathbf{v} = (v, r)$ with $v, r : \Lambda^{\rm hom} \to \mathbb{R}^d$ compactly supported,

$$\sum_{a\in\Lambda} \langle \delta\Phi_a(\mathbf{x}), \mathbf{v}\rangle = 0 \quad \text{and} \quad \sum_{a\in\Lambda} \big\langle \delta^2\Phi_a(\mathbf{x})\mathbf{v}, \mathbf{v}\big\rangle \geq c_0\big(|v|_{\mathscr{U}}^2 + \|r\|_{\ell^2}^2\big);$$

that is, the configuration must also be stable under perturbations of the shifts. This corresponds in fact to the classical notion of stability in complex lattices; see [7] and references therein.

Then we define the energy-difference functional

$$\mathscr{E}^{\rm a}(\mathbf{u}) := \sum_{a\in\Lambda} \Phi_a'(\mathbf{u}), \quad \text{where} \quad \Phi_a'(\mathbf{u}) := \Phi_a(\mathbf{x}+\mathbf{u}) - \Phi_a(\mathbf{x}).$$

It can again be shown that $\mathscr{E}^{\rm a}$ is well-defined and regular on the space [17]

$$\mathbf{U} := \big\{\mathbf{v} = (v, r) : \Lambda \to \mathbb{R}^{2d} \,\big|\, v \in \mathscr{U}, r \in \ell^2\big\}.$$

The exact atomistic problem now reads

$$\mathbf{u}^{\rm a} \in \arg\min\big\{\mathscr{E}^{\rm a}(\mathbf{u}) \,\big|\, \mathbf{u} \in \mathbf{U}\big\}.$$

4.3.2. The BGFC scheme. To define the BQCE and BGFC schemes, we first define the Cauchy–Born energy density by

$$\mathbf{W}(\mathsf{F}, p) := \det \mathsf{A}^{-1}\Phi_0^{\rm hom}\big((\mathsf{F}x, p)\big),$$

where $\Phi_a^{\rm hom}$ is the site energy potential for the defect-free lattice. Further, let $W'(\mathsf{G}, q) := W(\mathsf{I}+\mathsf{G}, p_0+q) - W(\mathsf{I}, p_0)$.

Let the computational geometry be set up precisely as in section 2.4, and let

$$\mathbf{U}_h := \big\{\mathbf{u}_h = (u_h, q_h) \,\big|\, u_h, q_h \in \mathscr{U}_h\big\}.$$

Note that, contrary to the usual practice, we require that both displacement and shift be continuous functions. This is necessary in order to be able to reconstruct atom positions. The BQCE energy functional, as proposed in [19], is given, for $\mathbf{u}_h = (u_h, q_h) \in \mathbf{U}_h$, by

$$\mathbf{E}^{\rm b}(\mathbf{u}_h) := \sum_{a\in\Lambda} (1-\beta(a))\Phi_a'(\mathbf{u}_h) + \int_{\Omega_h} Q_h\big[\beta W'(\nabla u_h, q_h)\big]\,{\rm d}x.$$

Because of the loss of point symmetry in the interaction potential, there is also a reduction in the accuracy of the Cauchy–Born model [7] and in the blending scheme. Indeed, the analysis in [19] suggests that the best possible error that can be expected for the complex lattice BQCE method is

$$\|\nabla\bar{u}^{\rm a} - \nabla u_h^{\rm b}\|_{L^2} + \|\bar{p}^{\rm a} - p_h^{\rm b}\|_{\ell^2} \lesssim \|\nabla\beta\|_{L^2} + \text{best approx. err.} + \text{CB err.};$$

that is, the blended ghost force error now scales like $\|\nabla\beta\|_{L^2}$. If $d = 2$, then it can be easily seen that $\|\nabla\beta\|_{L^2} \gtrsim 1$, while for $d = 3$, one even gets $\|\nabla\beta\|_{L^2} \gtrsim (R^{\rm a})^{1/2}$. Thus, the standard BQCE scheme cannot be optimized to become convergent in the energy-norm.

To formulate the BGFC scheme, we renormalize Φ_a and W a second time,

$$\Phi_a''(\mathbf{u}) := \Phi_a(\mathbf{x}+\mathbf{u}) - \Phi_a(\mathbf{x}) - \langle \delta\Phi_a(\mathbf{x}), \mathbf{u}\rangle, \quad \text{and}$$
$$\mathbf{W}''(\mathsf{G}, q) := W(\mathsf{I}+\mathsf{G}, p_0+q) - W(\mathsf{I}, p_0) - \partial_{\mathsf{F}} W(\mathsf{I}, p_0) : \mathsf{G} - \partial_p W(\mathsf{I}, p_0)\cdot q,$$

and define the BGFC energy functional

$$\mathbf{E}^{\rm bg}(\mathbf{u}) := \sum_{a\in\Lambda}(1-\beta(a))\Phi_a''(\mathbf{u}) + \int_{\Omega_h} Q_h\big[\beta W''(\nabla u, q)\big]\,{\rm d}x + \langle \mathbf{L}^{\rm ren}, \mathbf{u}\rangle,$$

where $\mathbf{L}^{\rm ren}$ is the linear functional correcting the forces in the defect core, defined analogously to $L^{\rm ren}$ in section 2.6. The BGFC scheme reads

$$\mathbf{u}_h^{\rm bg} \in \arg\min\big\{\mathbf{E}^{\rm bg}(\mathbf{v}) \,\big|\, \mathbf{v}\in\mathbf{U}_h\big\}. \tag{4.2}$$

4.3.3. Convergence rate. While we leave a rigorous convergence theory for (4.2) to future work, we can still speculate what rate of convergence may be expected.

Arguing analogously to sections 2.6 and 5, we now observe that the error due to the blended ghost forces can be bounded by

$$\|\nabla\bar{u}^{\rm a} - \nabla u_h^{\rm bg}\|_{L^2} + \|\bar{p}^{\rm a} - p_h^{\rm bg}\|_{L^2} \lesssim \|\nabla\beta\|_{L^\infty}\big(\|\nabla\bar{u}^{\rm a}\|_{L^2(\Omega^{\rm b})} + \|\bar{p}^{\rm a}\|_{L^2(\Omega^{\rm b})}\big) + \text{best approx. err.} + \text{Cauchy–Born err.}$$

It is reasonable to expect that the regularity for the deformation fields y_1, y_2 is similar as for simple lattices (indeed, this is the premise of the complex lattice Cauchy–Born rule) and therefore the best approximation error is of the same order, i.e., $(R^{\rm a})^{-d}$. The Cauchy–Born modeling error can also be bounded by $\|\nabla^2\tilde{u}^{\rm a}\|_{L^2(\mathbb{R}^d\setminus B_{R^{\rm a}})} + \|\nabla\tilde{p}^{\rm a}\|_{L^2(\mathbb{R}^d\setminus B_{R^{\rm a}})} \lesssim (R^{\rm a})^{-d}$, where we assumed again the same regularity for complex lattice displacement fields as that for the simple-lattice case. (Since the shift itself is a gradient, it is reasonable to expect that $\nabla\tilde{p}^{\rm a}$ decays like a second gradient.)

Thus, we are left to discuss the error due to the ghost forces. Assuming the typical decay for point defects, $|\nabla\tilde{u}^{\rm a}| + |\tilde{p}^{\rm a}| \lesssim |x|^{-d}$, we obtain that for a quasi-optimal choice of β, satisfying $\|\nabla\beta\|_{L^\infty} \lesssim (R^{\rm b} - R^{\rm a})^{-1}$,

$$\|\nabla\beta\|_{L^\infty}\big(\|\nabla\bar{u}^{\rm a}\|_{L^2(\Omega^{\rm b})} + \|\bar{p}^{\rm a}\|_{L^2(\Omega^{\rm b})}\big) \lesssim (R^{\rm b}-R^{\rm a})^{-1}(R^{\rm a})^{-d/2}.$$

Upon choosing $R^{\rm b} - R^{\rm a} \approx R^{\rm a}$, this yields the rates

$$\|\nabla\beta\|_{L^\infty}\big(\|\nabla\bar{u}^{\rm a}\|_{L^2(\Omega^{\rm b})} + \|\bar{p}^{\rm a}\|_{L^2(\Omega^{\rm b})}\big) \lesssim \begin{cases} (R^{\rm a})^{-2}, & d=2,\\ (R^{\rm a})^{-5/2}, & d=3,\end{cases}$$

which are the best approximation rate for $d = 2$ and a slightly reduced rate for $d = 3$. We therefore conclude that the expected rate of convergence for the complex lattice BGFC scheme, for point defects, is

$$\|\nabla\bar{u}^{\rm a} - \nabla u_h^{\rm bg}\|_{L^2} + \|\bar{p}^{\rm a} - p_h^{\rm bg}\|_{\ell^2} \lesssim \begin{cases} (R^{\rm a})^{-2} \approx ({\rm DOF})^{-1}, & d=2,\\ (R^{\rm a})^{-5/2} \approx ({\rm DOF})^{-5/6}, & d=3.\end{cases}$$

With these heuristics in mind, we expect that it would be feasible to generalize the analysis in [10] and section 5 and thus obtain the first rigorously convergent a/c coupling scheme for complex crystals.

5. Analysis. For our rigorous error estimates we focus on a simplified point defect problem, following [10]. We shall cite several results that are summarized in [10] but drawn from other sources, but for the sake of convenience we will only cite [10] as a reference. A range of generalizations are possible but require some additional work, and in particular a more complex notation.

We assume $\Lambda \equiv \Lambda^{\rm hom} \equiv \mathbb{Z}^d$ (a deformation of the lattice can be absorbed into the potential), with globally homogeneous site energies with finite interaction radius in *reference configuration*. That is, we assume that there exists $\mathcal{R} \subset B_{r_{\rm cut}} \cap (\Lambda \setminus \{0\})$, finite, and $V \in C^4((\mathbb{R}^d)^{\mathcal{R}})$ such that $\Phi_a(y) = V(Dy(a))$, where $Dy(a) := (D_\rho y(a))_{\rho\in\mathcal{R}}$ and $D_\rho y(a) := y(a+\rho) - y(a)$. We assume throughout that V is point symmetric, i.e., $-\mathcal{R} = \mathcal{R}$ and $V((-g_{-\rho})) = V((g_\rho))$ for all $(g_\rho)_{\rho\in\mathcal{R}} \in (\mathbb{R}^d)^{\mathcal{R}}$.

A defect is introduced by adding an external potential $\mathscr{P}^{\rm def} \in C^2(\mathscr{U})$, which depends only on $Du(a), |a| < R^{\rm def}$. The atomistic problem (2.3) now reads

$$u^{\rm a} \in \arg\min \big\{ \mathscr{E}^{\rm a}(v) + \mathscr{P}^{\rm def}(v) \,\big|\, v \in \mathscr{U} \big\}. \tag{5.1}$$

We call $u^{\rm a}$ a strongly stable solution to (5.1) if there exists $\gamma > 0$ such that

$$\langle \delta[\mathscr{E}^{\rm a} + \mathscr{P}^{\rm def}](u^{\rm a}), v\rangle = 0 \quad \text{and} \quad \langle \delta^2[\mathscr{E}^{\rm a} + \mathscr{P}^{\rm def}](u^{\rm a})v, v\rangle \geq \gamma |v|^2_{\mathscr{U}} \quad \forall v \in \mathscr{U}.$$

The BGFC approximation to (5.1) is given by

$$u_h^{\rm bg} \in \arg\min \big\{ \mathscr{E}^{\rm bg}(v_h) + \mathscr{P}^{\rm def}(v_h) \,\big|\, v_h \in \mathscr{U}_h \big\}, \tag{5.2}$$

using the notation of section 2.6.

5.1. Additional assumptions. We now summarize the main assumptions required to state rigorous convergence results. All assumptions can be satisfied in practice and are discussed in detail in [10].

We assume that $\beta \in C^{2,1}(\mathbb{R}^d)$, $0 \leq \beta \leq 1$. Let $r'_{\rm cut} := 2r_{\rm cut} + \sqrt{d}$, $\Omega^{\rm a} := {\rm supp}(1-\beta) + B_{r'_{\rm cut}}$, $\Omega^{\rm b} := {\rm supp}(\nabla\beta) + B_{r'_{\rm cut}}$ and $\Omega^{\rm c} := ({\rm supp}(\beta) + B_{r'_{\rm cut}}) \cap \Omega_h$. Then we require that there exist radii $R^{\rm a} \leq R^{\rm b} \leq R^{\rm c}$ and constants $C_{\rm b}, C_\Omega$ such that

$$\begin{aligned}
&R^{\rm b} \leq C_{\rm b} R^{\rm a}, \qquad \|\nabla^j \beta\|_{L^\infty} \leq C_{\rm b} (R^{\rm a})^{-j},\ j = 1,2,3;\\
&{\rm supp}(\beta) \supset B_{R^{\rm a} + r'_{\rm cut}}, \qquad {\rm supp}(1-\beta) \subset B_{R^{\rm b} - r'_{\rm cut}};\\
&B_{R^{\rm c}} \subset \Omega^{\rm a} \cup \Omega^{\rm c} \quad \text{and} \quad R^{\rm c} \geq C_\Omega (R^{\rm a})^{1+d/2}.
\end{aligned}$$

To state the final assumption that we require on $\mathcal{T}_h$, we first need to define a piecewise affine interpolant of lattice functions. If $d = 2$, let $\hat{\mathcal{T}} := \{\hat{T}_1, \hat{T}_2\}$, where $\hat{T}_1 = {\rm conv}\{0, e_1, e_2\}$ and $\hat{T}_2 = {\rm conv}\{e_1, e_2, e_1 + e_2\}$, where conv denotes the convex hull of a set of points. If $d = 3$, let $\hat{\mathcal{T}} := \{\hat{T}_1, \dots, \hat{T}_6\}$ be the standard subdivision of $[0,1]^3$ into six tetrahedra (see [10, Fig. 1]). Then $\mathcal{T} := \bigcup_{\ell\in\Lambda} (\ell + \hat{\mathcal{T}})$ defines a regular and uniform triangulation of $\mathbb{R}^d$ with node set Λ. For each $v : \Lambda \to \mathbb{R}^m$, there exists a unique $\bar{v} \in C(\mathbb{R}^d; \mathbb{R}^m)$ such that $\bar{v}(\ell) = v(\ell)$ for all $\ell \in \Lambda$. In particular, we note that the seminorms $\|\nabla \bar{v}\|_{L^2}$ and $|v|_{\mathscr{U}}$ are equivalent.

Our final requirement on the approximation parameters is that there exists a constant C_h such that

$$\begin{aligned}
&\mathcal{T}_h \cap \Omega^{\rm a} \equiv \mathcal{T} \cap \Omega^{\rm a}, \qquad\qquad \max_{T\in\mathcal{T}_h} h_T^d / |T| \leq C_h,\\
&h(x) \leq C_h \max\big(1, |x|/R^{\rm a}\big) \quad \text{and} \quad \#\mathcal{T}_h \leq C_h (R^{\rm a})^d \log(R^{\rm a}).
\end{aligned}$$

By $\mathcal{T}_h \cap \Omega^{\rm a} \equiv \mathcal{T} \cap \Omega^{\rm a}$ we mean that if $T \in \mathcal{T}, T \cap \Omega^{\rm a} \neq \emptyset$, then $T \in \mathcal{T}_h$ (and hence also vice versa). The condition $h(x) \leq C_h \max\big(1, |x|/R^{\rm a}\big)$ can be weakened as in the foregoing sections (see, e.g., [14, 21]), but for consistency with [10] we chose this more restrictive coarsening for our analysis.

We remark that $(\beta, \mathcal{T}_h)$ are the main approximation parameters, while the "regularity constants" $\mathbf{C} = (C_{\rm b}, C_h, C_\Omega)$ are "derived parameters." In the following we *fix* the constants $\mathbf{C}$ to some given bounds, and admit any pair $(\beta, \mathcal{T}_h)$ satisfying the foregoing conditions with these constants. When we write $A \lesssim B$, we mean that there exists a constant C depending only on $\mathbf{C}$ (as well as on the solution and on the model) but not on $(\beta, \mathcal{T}_h)$ such that $A \leq CB$.

5.2. Convergence result. The following convergence result is a direct extension of Theorem 3.1, Proposition 3.2, and Theorem 3.3 in [10] to the BGFC method. The proof of the theorem is given in the next two sections.

THEOREM 5.1. *Let $u^{\rm a}$ be a strongly stable solution to* (5.1)*; then for any given set of constants $\mathbf{C}$ there exist $C, C', R_0^{\rm a} > 0$ such that, for all $(\beta, \mathcal{T}_h)$ satisfying the conditions of section* 5.1*, and in addition $R^{\rm a} \geq R_0^{\rm a}$, there exists a solution $u_h^{\rm bg}$ to* (5.2) *such that*

$$\|\nabla \bar{u}^{\rm a} - \nabla u_h^{\rm bg}\|_{L^2} \leq C(R^{\rm a})^{-d/2-1} \leq C'\big(\tfrac{\log \#\mathcal{T}_h}{\#\mathcal{T}_h}\big)^{1/2+1/d}, \tag{5.3}$$

$$\big|\mathscr{E}^{\rm a}(u^{\rm a}) - \mathscr{E}^{\rm bg}(u_h^{\rm bg})\big| \leq C(R^{\rm a})^{-d-2} \leq C'\big(\tfrac{\log \#\mathcal{T}_h}{\#\mathcal{T}_h}\big)^{1+2/d}. \tag{5.4}$$

Remark 3. (1) The only assumption we made that represents a genuine restriction of generality is that $\|\nabla^j \beta\|_{L^\infty} \lesssim (R^{\rm a})^{-j}$. We require this to prove stability of the BQCE and BGFC schemes.

(2) However, the proof of (5.4) shows that the energy error would be suboptimal if we were to choose a narrower blending region (and thus a slower rate of $\|\nabla^j \beta\|_{L^\infty} \lesssim (R^{\rm a})^{-sj}$ for some $s < 1$). This appears to contradict our numerical results in section 3 and suggests that the energy error estimate may be suboptimal.

5.3. Proof of the energy-norm error estimate. To prove the result we will need to refer to another technical tool from [10], namely a $C^{2,1}$-conforming multiquintic, which we use to measure the regularity of an atomistic displacement.

For $v : \Lambda \to \mathbb{R}^m$ and $i = 1, \ldots, d$, let $\mathsf{d}_i^0 v(\ell) := v(\ell)$; $\mathsf{d}_i^1 v(\ell) := \frac{1}{2}(u(\ell + e_i) - u(\ell - e_i))$ and $\mathsf{d}_i^2 v(\ell) := u(\ell + e_i) - 2u(\ell) + u(\ell - e_i)$. Lemma 2.1 in [10] states that for each $\ell \in \Lambda$ there exists a unique multiquintic function $\tilde{v} : \ell + [0,1]^d \to \mathbb{R}^m$ defined through the conditions

$$\partial_{x_1}^{\alpha_1} \cdots \partial_{x_d}^{\alpha_d} \tilde{v}(\ell') = \mathsf{d}_1^{\alpha_1} \cdots \mathsf{d}_d^{\alpha_d} v(\ell') \quad \forall \ell' \in \ell + \{0,1\}^d,\ \alpha \in \{0,1,2\}^d,\ \|\alpha\|_\infty \leq 2,$$

and, moreover, that the resulting piecewise defined function $\tilde{v} \in C^{2,1}(\mathbb{R}^d; \mathbb{R}^m)$.

We begin the proof of Theorem 5.1 by noting that the renormalized site energy potential

$$V''(Du) := V(\mathcal{R} + Du) - V(\mathcal{R}) - \langle \delta V(\mathcal{R}), Du \rangle$$

is an admissible potential for [10, Thm. 3.1]. Further, the conditions we put forward in section 5.1 are precisely those needed to apply [10, Thm. 3.1] with V replaced by V'', thus treating BGFC as a simple BQCE method. Hence, we obtain that, under the conditions of Theorem 5.1, there exist a solution $u_h^{\rm bg}$ to (5.2) and constants C_1, C_2

depending only on $\mathbf{C}$, but independent of the approximation parameters, such that

$$\|\nabla \bar{u}^{\rm a} - \nabla u_h^{\rm bg}\|_{L^2} \le C_1 \|\nabla^2 \beta\|_{L^2} + C_2 \Big(\|\nabla \bar{u}^{\rm a}\|_{L^2(\mathbb{R}^2 \setminus B_{R^{\rm c}/2})} + \|h \nabla^2 \tilde{u}^{\rm a}\|_{L^2(\Omega^{\rm c})} + \|h^2 \nabla^3 \tilde{u}^{\rm a}\|_{L^2(\Omega^{\rm c})} + \|\nabla^2 \tilde{u}^{\rm a}\|_{L^4(\Omega^{\rm c})}^2 \Big). \tag{5.5}$$

Here we did not write out some terms that are trivially dominated by those that we did write. In the following we write $u \equiv u^{\rm a}$.

The group preceded by the constant C_2 cannot be further improved, but we will analyze in more detail the group $C_1 \|\nabla^2 \beta\|_{L^2}$. This term arises from both the coarsening and modeling error analyses of the BQCE scheme in sections 6.1 and 6.2 of [10] (see also the summary in section 4.3 of [10]). We will now analyze this group in more detail.

To avoid rewriting all the terms arising in the consistency analysis in [10], we will now directly refer to the notation of that paper. The terms on the right-hand side of (5.5) all arise from bounding above the terms $\mathrm{T}_1, \dots, \mathrm{T}_4$ defined at the beginning of [10, sect. 6.1]. In [10, Lems. 6.1 and 6.2], analyzing the coarsening error contributions, it is shown that

$$\begin{aligned} &|\mathrm{T}_1| + |\mathrm{T}_2| + |\mathrm{T}_3| \lesssim \epsilon_\beta^{\rm coarse} + \epsilon_h^{\rm cb}, \quad \text{where} \\ &\epsilon_\beta^{\rm coarse} = \|\partial W''(\mathsf{I} + \nabla \tilde{u}) \nabla^2 \beta\|_{L^2} \quad \text{and} \\ &\epsilon_h^{\rm cb} = C_2 \big(\|\nabla \bar{u}\|_{L^2(\mathbb{R}^2 \setminus B_{R^{\rm c}/2})} + \|h \nabla^2 \tilde{u}\|_{L^2(\Omega^{\rm c})} + \|h^2 \nabla^3 \tilde{u}\|_{L^2(\Omega^{\rm c})} + \|\nabla^2 \tilde{u}\|_{L^4(\Omega^{\rm c})}^2 \big), \end{aligned} \tag{5.6}$$

and we assumed, without loss of generality, that the test function is normalized. Using the fact that $\partial W''(\mathsf{I}) = 0$ (due to the renormalization, the reference configuration is now stress free) we therefore obtain

$$\epsilon_\beta^{\rm coarse} = \big\| \big[\partial W''(\mathsf{I} + \nabla \tilde{u}) - \partial W''(\mathsf{I}) \big] \nabla^2 \beta \big\|_{L^2} \lesssim \big\| \, |\nabla \tilde{u}| \, |\nabla^2 \beta| \, \big\|_{L^2}. \tag{5.7}$$

We now turn towards the modeling error contribution. Assuming again, without loss of generality, that the test function is normalized, we have

$$|\mathrm{T}_4| \lesssim \|\mathsf{R}^\beta\|_{L^2},$$

and R^β is a stress error function defined in [10, eq. (4.23)], but with V replaced by V''. Following the proof of [10, Lem. 6.4] we see that in [10, eq. (6.6)] it splits

$$|\mathsf{R}^\beta(x)| \le |T_1| + |T_2| + O(\epsilon_2^2)$$

(note the abuse of notation: these are *different* T_1, T_2 groups than in (5.6)), and it estimates $|T_2| + O(\epsilon_2^2) \lesssim \epsilon_h^{\rm cb}$. The last term is given by

$$T_1 = \beta \partial W'' - \sum_{\ell \in \Lambda} \beta(\ell) \sum_{\rho \in \mathcal{R}} \big[V''_{,\rho} \otimes \rho \big] \omega_\rho(\ell - x),$$

where $\partial W'' = \partial W''(\mathsf{I} + \nabla \tilde{u}(x))$, $V''_{,\rho} = V''_{,\rho}((\mathsf{I} + \nabla \tilde{u}(x))\mathcal{R})$, and $\omega_\rho(y) = \int_{s=0}^1 \bar{\zeta}(y + s\rho) \, {\rm d}s$, with $\bar{\zeta}$ being the P1 hat function for the origin on the mesh $\mathcal{T}$. The $O(\|\nabla^2 \beta\|)$ term now arises by expanding β,

$$\beta(\ell) = \beta(x) + \nabla \beta(x) \cdot (\ell - x) + r_\beta(x; \ell),$$

with $|r_\beta(x;\ell)| \lesssim \|\nabla^2\beta\|_{L^\infty}$ due to the fact that only ℓ within a fixed radius around x are considered in the seemingly infinite sum. The contribution from the term $\nabla\beta(x)\cdot(\ell - x)$ in T_1 vanishes due to the point symmetry assumption; see the proof of [10, Lem. 6.4] for more details. Exploiting also the fact that $V''_{,\rho}(\mathcal{R}) \equiv 0$ and $\sum_{\ell\in\Lambda}\omega_\rho(\ell - x) = 1$ (see [10, eq. (4.18)]), and bounding several terms above by $\epsilon_h^{\rm cb}$, we obtain

$$\begin{aligned}
|T_1| &\le \|\nabla^2\beta\|_{L^\infty}\sum_{\rho\in\mathcal{R}}\Big|\big(V''_{,\rho}(\mathcal{R}+\nabla\tilde{u}) - V''_{,\rho}(\mathcal{R})\big)\otimes\rho\sum_{\ell\in\Lambda}\omega_\rho(\ell - x)\Big| + \epsilon_h^{\rm cb}\\
&\lesssim \|\nabla^2\beta\|_{L^\infty}\sum_{\rho\in\mathcal{R}}\big|V''_{,\rho}(\mathcal{R}+\nabla\tilde{u}) - V''_{,\rho}(\mathcal{R})\big| + \epsilon_h^{\rm cb}\\
&\lesssim \|\nabla^2\beta\|_{L^\infty}|\nabla\tilde{u}(x)| + \epsilon_h^{\rm cb}.
\end{aligned}$$

Note that T_1 is a function of x. The improved modeling error estimate is obtained by taking the L^2-norm of T_1. Upon noting that $T_1(x) = 0$ outside $\Omega^{\rm b}$, we therefore obtain

$$|\mathrm{T}_4| \lesssim \epsilon_\beta^{\rm model} + \epsilon_h^{\rm cb} \lesssim \|\nabla^2\beta\|_{L^\infty}\|\nabla\tilde{u}\|_{L^2(\Omega^{\rm b})} + \epsilon_h^{\rm cb}. \tag{5.8}$$

Combining (5.6), (5.7), and (5.8) we arrive at

$$\begin{aligned}
\|\nabla\bar{u} - \nabla u_h^{\rm bg}\|_{L^2} \le C\Big(&\|\nabla^2\beta\|_{L^\infty}\|\nabla\tilde{u}\|_{L^2(\Omega^{\rm b})} + \|\nabla\bar{u}\|_{L^2(\mathbb{R}^2\setminus B_{R^{\rm c}/2})} + \|h\nabla^2\tilde{u}\|_{L^2(\Omega^{\rm c})}\\
&+ \|h^2\nabla^3\tilde{u}\|_{L^2(\Omega^{\rm c})} + \|\nabla^2\tilde{u}\|^2_{L^4(\Omega^{\rm c})}\Big),
\end{aligned} \tag{5.9}$$

for a constant C that depends only on $\mathbf{C}$, but is independent of $(\beta, \mathcal{T}_h)$.

Following the proof of [10, Thm. 3.3], in section 3.2.2 of [10] it is straightforward now to obtain the rate (5.3). Towards its proof we only remark that according to [10, Lem. 2.3], $|\nabla\tilde{u}(x)| \lesssim |x|^{-d}$, and hence using the assumption $\|\nabla^2\beta\|_{L^\infty} \lesssim (R^{\rm a})^{-2}$, we obtain

$$\|\nabla^2\beta\|_{L^\infty}\,\|\nabla\tilde{u}\|_{L^2(\Omega^{\rm b})} \lesssim (R^{\rm a})^{-2}\bigg(\int_{R^{\rm a}}^{R^{\rm b}} r^{d-1}r^{-2d}\,\mathrm{d}r\bigg)^{1/2} \lesssim (R^{\rm a})^{-2-d/2}.$$

This completes the proof of (5.3).

5.4. Proof of the energy error estimate. As in the case of the energy-norm error estimate, we only modify some specific parts of the proof for the BQCE case in section 6.3 of [10], as required to obtain the improved energy error estimate. To follow the notation let $u \equiv u^{\rm a}$ and $u_h \equiv u_h^{\rm bg}$. Further, we recall that $\Pi_h u \in \mathscr{U}_h$ is a best approximation of u. For the following proof we do not need to know its precise definition, but only remark that $\Pi_h u = u$ in $\Omega^{\rm a}$, and, as an intermediate step in the proof of (5.3), one obtains

$$\|\nabla\tilde{u} - \nabla\Pi_h u\|_{L^2(\Omega^{\rm c})} + \|\nabla u_h - \nabla\Pi_h u\|_{L^2} \lesssim (R^{\rm a})^{-1-d/2}.$$

Following the proof of the BQCE energy error estimate in section 6.3 of [10], we split the energy error into $\mathscr{E}^{\rm a}(u) - \mathscr{E}^{\rm bg}(u_h) = T_1 + T_2 + T_3$, where

$$T_1 = \mathscr{E}^{\rm a}(u) - \tilde{\mathcal{E}}, \qquad T_2 = \tilde{\mathcal{E}} - \mathscr{E}^{\rm bg}(\Pi_h u), \qquad T_3 = \mathscr{E}^{\rm bg}(\Pi_h u) - \mathscr{E}^{\rm bg}(u_h),$$
$$\text{and} \quad \tilde{\mathcal{E}} = \sum_{\ell\in\Lambda}(1-\beta(\ell))V''(Du(\ell)) + \int_{\mathbb{R}^d}[Q_h\beta]W''(\nabla\tilde{u})\,\mathrm{d}x.$$

We treat the terms in the same order as in [10].

As in [10], the term T_3 can be bounded by

$$|T_3| \lesssim \|\nabla u_h - \nabla \Pi_h u\|_{L^2}^2 \lesssim (R^{\rm a})^{-2-d}. \tag{5.10}$$

The term T_1 is split further into

$$\begin{aligned} T_1 &= \sum_{\ell\in\Lambda} \beta(\ell)\big(V''(Du(\ell)) - W''(\nabla\tilde{u}(\ell))\big) \\ &\quad - \int_{\mathbb{R}^d} \big([Q_h\beta]W''(\nabla\tilde{u}) - I_1[\beta W''(\nabla\tilde{u})]\big)\,{\rm d}x =: T_{1,1} + T_{1,2}, \end{aligned}$$

where I_1 denotes the P1 nodal interpolant for the atomistic mesh $\mathcal{T}$. The second term is essentially a quadrature error, and following the proof of (6.12) in [10] (but noting that the inverse-estimate trick for β is not required in our present setting), it is easy to see that

$$|T_{1,2}| \lesssim \sum_{T\in\mathcal{T}} \|\nabla^2[\beta W''(\nabla\tilde{u})]\|_{L^\infty(T)}.$$

The summand vanishes, unless $T \subset \Omega^{\rm c}$. In the latter case, we have

$$\begin{aligned} \|\nabla^2[\beta W''(\nabla\tilde{u})]\|_{L^\infty(T)} &\lesssim \|\nabla^2\beta\|_{L^\infty}\|\nabla\tilde{u}\|_{L^\infty(T)}^2 + \|\nabla\beta\|_{L^\infty(T)}\|\partial W''(\nabla\tilde{u})\nabla^2\tilde{u}\|_{L^\infty(T)} \\ &\quad + \|\partial W''(\nabla\tilde{u})\nabla^3\tilde{u}\|_{L^\infty} + \|\partial^2 W''(\nabla\tilde{u})|\nabla^2\tilde{u}|^2\|_{L^\infty(T)} \\ &\lesssim \|\nabla^2\beta\|_{L^\infty}\|\nabla\tilde{u}\|_{L^2(T)}^2 + \|\nabla\beta\|_{L^\infty}\|\nabla\tilde{u}\|_{L^2(T)}\|\nabla^2\tilde{u}\|_{L^2(T)} \\ &\quad + \|\nabla\tilde{u}\|_{L^2(T)}\|\nabla^3\tilde{u}\|_{L^2(T)} + \|\nabla^2\tilde{u}\|_{L^2(T)}^2. \end{aligned}$$

Therefore, we obtain

$$\begin{aligned} |T_{1,2}| &\lesssim \|\nabla^2\beta\|_{L^\infty}\|\nabla\tilde{u}\|_{L^2(\Omega^{\rm b})}^2 + \|\nabla\beta\|_{L^\infty}\|\nabla\tilde{u}\|_{L^2(\Omega^{\rm b})}\|\nabla^2\tilde{u}\|_{L^2(\Omega^{\rm b})} \\ &\quad + \|\nabla\tilde{u}\|_{L^2(\Omega^{\rm c})}\|\nabla^3\tilde{u}\|_{L^2(\Omega^{\rm c})} + \|\nabla^2\tilde{u}\|_{L^2(\Omega^{\rm c})}^2 \\ &\lesssim (R^{\rm a})^{-2-d} + (R^{\rm a})^{-2-d} + (R^{\rm a})^{-2-d} + (R^{\rm a})^{-2-d} \approx (R^{\rm a})^{-2-d}. \end{aligned} \tag{5.11}$$

To estimate $T_{1,1}$ we begin by noting that

$$\begin{aligned} V''(Du) - W''(\nabla u) &= V''(\mathcal{R} + Du) - V''(\mathcal{R} + \nabla_{\mathcal{R}} u) \\ &= \langle \delta V''(\mathcal{R} + \nabla_{\mathcal{R}} u), Du - \nabla_{\mathcal{R}} u\rangle \\ &\quad + \langle \delta^2 V(\Theta)(Du - \nabla_{\mathcal{R}} u), Du - \nabla_{\mathcal{R}} u\rangle, \end{aligned}$$

where $\Theta \in {\rm conv}\{\mathcal{R}+Du, \mathcal{R}+\nabla_{\mathcal{R}}u\}$ and $\nabla_{\mathcal{R}}u := (\nabla_\rho u)_{\rho\in\mathcal{R}}$. Then, continuing to argue as in [10, Lem. 6.6] (performing a Taylor expansion on Du, using point symmetry of V'', and in particular exploiting the fact that $\|\delta V''(\mathcal{R} + \nabla_{\mathcal{R}} u)\| \lesssim |\nabla\tilde{u}|$) we obtain

$$\begin{aligned} \big|\langle \delta V''(\mathcal{R} + \nabla_{\mathcal{R}} u), Du - \nabla_{\mathcal{R}} u\rangle\big| &\lesssim \|\nabla\tilde{u}\|_{L^\infty(\nu_x)}\|\nabla^3\tilde{u}\|_{L^\infty(\nu_x)}, \\ \big|\langle \delta^2 V(\Theta)(Du - \nabla_{\mathcal{R}} u), Du - \nabla_{\mathcal{R}} u\rangle\big| &\lesssim \|\nabla^2\tilde{u}\|_{L^\infty(\nu_x)}^2, \end{aligned}$$

where $\nu_x = B_{r'_{\rm cut}}(x)$. Using the fact that $\nabla^3\tilde{u}$ is a piecewise polynomial we can use the inverse inequalities in (5.7) of [10] to obtain, as in (6.14) of [10], that

$$\begin{aligned} |T_{1,1}| &\lesssim \|\nabla\tilde{u}\|_{L^2(\Omega^{\rm c})}\|\nabla^3\tilde{u}\|_{L^2(\Omega^{\rm c})} + \|\nabla^2\tilde{u}\|_{L^2(\Omega^{\rm c})}^2 \\ &\lesssim (R^{\rm a})^{-2-d} + (R^{\rm a})^{-2-d} \approx (R^{\rm a})^{-2-d}. \end{aligned} \tag{5.12}$$

Since $\Pi_h u = u$ in $\Omega^{\rm a}$, the term T_2 simplifies to

$$T_2 = \int_{\mathbb{R}^d} [Q_h\beta]\big(W''(\nabla\tilde{u}) - W''(\nabla\tilde{u} - \nabla e)\big)\Big)\,\mathrm{d}x,$$

where $e := \tilde{u} - \Pi_h u$ and we used the fact that $Q_h[\beta W''(\nabla\Pi_h u)] = [Q_h\beta]W''(\nabla\Pi_h u)$. We begin by expanding $W''(\nabla\tilde{u}) - W''(\nabla\tilde{u} - \nabla e) = \partial W''(\nabla\tilde{u}) : \nabla e + O(|\nabla e|^2)$ to obtain

$$\begin{aligned} T_2 &\lesssim \left| \int_{\mathbb{R}^d} [Q_h\beta]\big[\partial W''(\nabla\tilde{u}) : \nabla e\big]\,\mathrm{d}x \right| + \|\nabla e\|^2_{L^2(\Omega^{\rm c})} \\ &\lesssim \left| \int_{\mathbb{R}^d} \beta\big[\partial W''(\nabla\tilde{u}) : \nabla e\big]\,\mathrm{d}x \right| + \left| \int_{\mathbb{R}^d} [Q_h\beta - \beta]\big[\partial W''(\nabla\tilde{u}) : \nabla e\big]\,\mathrm{d}x \right| \\ &\quad + \|\nabla e\|^2_{L^2(\Omega^{\rm c})} \lesssim T_{2,1} + T_{2,2} + T_{2,3}. \end{aligned}$$

To treat $T_{2,1}$ we integrate by parts, and then use $|\partial W''(\nabla\tilde{u})| = |\partial W(\mathsf{I}+\nabla\tilde{u}) - \partial W(\mathsf{I})| \lesssim |\nabla\tilde{u}|$, $\|e\|_{L^2(T)} \lesssim \|h^2\nabla^2\tilde{u}\|_{L^2(T)}$, and $\|h^2\nabla^2\tilde{u}\|_{L^2(\Omega^{\rm c})} \lesssim (R^{\rm a})^{-1-d/2}$ to estimate

$$\begin{aligned} T_{2,1} &= \left| \int_{\mathbb{R}^d} -\mathrm{div}\Big(\beta\partial W''(\nabla\tilde{u})\Big)\cdot e\,\mathrm{d}x \right| \\ &\lesssim \|\nabla\beta\|_{L^\infty}\|\partial W''(\nabla\tilde{u})\|_{L^2(\Omega^{\rm c})}\|e\|_{L^2(\Omega^{\rm c})} + \|\nabla^2\tilde{u}\|_{L^2(\Omega^{\rm c})}\|e\|_{L^2(\Omega^{\rm c})} \\ &\lesssim \|\nabla\beta\|_{L^\infty}\|\nabla\tilde{u}\|_{L^2(\Omega^{\rm c})}\|e\|_{L^2(\Omega^{\rm c})} + \|\nabla^2\tilde{u}\|_{L^2(\Omega^{\rm c})}\|e\|_{L^2(\Omega^{\rm c})} \\ &\lesssim (R^{\rm a})^{-1}(R^{\rm a})^{-d/2}(R^{\rm a})^{-1-d/2} + (R^{\rm a})^{-1-d/2}(R^{\rm a})^{-1-d/2} \approx (R^{\rm a})^{-2-d}. \end{aligned}$$

The terms $T_{2,2}$ and $T_{2,3}$ are estimated analogously, by $T_{2,j} \lesssim (R^{\rm a})^{-2-d}$, $j = 2, 3$, and thus we obtain that

$$|T_2| \lesssim (R^{\rm a})^{-2-d}. \tag{5.13}$$

Combining (5.10), (5.11), (5.12), and (5.13) completes the proof of (5.4).

6. Analysis of the extension to P2-FEM. In section 4.1 we discussed the P2-BGFC extension of the BGFC method to employ (second-order) P2 finite elements in the continuum region. In this section, we state a rigorous convergence result for the P2-BGFC method, for the model problem from section 5.

6.1. Notation and assumptions. We adopt the notation and assumptions from sections 5 and 5.1, with the only exception that instead of $R^{\rm c} \geq C_\Omega(R^{\rm a})^{1+2/d}$, we now require that

$$R^{\rm c} \geq C_\Omega(R^{\rm a})^{1+4/d}.$$

Moreover, we slightly modify the P2-BGFC formulation by decomposing $\mathcal{T}_h = \mathcal{T}_h^{(\mathrm{P1})} \cup \mathcal{T}_h^{(\mathrm{P2})}$, where

$$\mathcal{T}_h^{(\mathrm{P1})} := \big\{T \in \mathcal{T}_h \,\big|\, T \cap \Omega^{\rm a} \neq \emptyset\big\},$$

which defines the solution space $\mathscr{U}_h^{(2)}$ via (4.1). The quadrature operator Q_h is now defined, for $f \in C(\Omega_h)$, by

$$Q_h f = \sum_{T\in\mathcal{T}_h^{(\mathrm{P1})}} \chi_T Q_T^{(1)} f + \sum_{T\in\mathcal{T}_h^{(\mathrm{P2})}} \chi_T Q_T^{(2)} f,$$

where $Q_T^{(1)}$ is the element midpoint interpolant and $Q_T^{(2)}$ is the piecewise affine interpolant at the element face midpoints. Note that $Q_T^{(1)}$ is second-order, while $Q_T^{(2)}$ is third-order; that is, $Q_T^{(2)}$ integrates quadratic functions exactly. With this notation, the P2-BGFC energy functional is given by

$$\mathscr{E}^{\rm bg2}(u_h) := \sum_{\ell\in\Lambda}(1-\beta(\ell))V(Du_h(\ell)) + \int_{\Omega_h} Q_h\big[\beta W(\nabla u_h)\big]\,{\rm d}x,$$

and the P2-BGFC model problem reads

$$u_h^{\rm bg2} \in \arg\min\big\{\mathscr{E}^{\rm bg2}(v_h) + \mathscr{P}^{\rm def}(v_h)\,\big|\,v_h\in\mathscr{U}_h^{(2)}\big\}. \tag{6.1}$$

6.2. Statement of the result. The following result is an extension of Theorem 5.1 to the P2-BGFC method. Its proof is largely an immediate extension of the proofs of Theorem 5.1 and of the analysis in [10]; however, there is one subtle point concerning the second-order consistency that must be addressed with care; see section 6.6.1.

THEOREM 6.1. *Let $u^{\rm a}$ be a strongly stable solution to* (5.1)*; then for any given set of constants* $\mathbf{C}$ *there exist $C, C', R_0^{\rm a} > 0$ such that, for all $(\beta, \mathcal{T}_h)$ satisfying the conditions of section* 5.1*, and in addition $R^{\rm a} \geq R_0^{\rm a}$ and $R^{\rm c} \geq C_\Omega (R^{\rm a})^{1+4/d}$, there exists a solution $u_h^{\rm bg2}$ to* (5.2) *such that*

$$\|\nabla \bar{u}^{\rm a} - \nabla u_h^{\rm bg2}\|_{L^2} \leq C(R^{\rm a})^{-d/2-2} \leq C'\left(\frac{\log \#\mathcal{T}_h}{\#\mathcal{T}_h}\right)^{1/2+2/d}. \tag{6.2}$$

The proof heavily builds on [10]. The required modifications for Theorem 6.1 are presented in sections 6.3–6.6.

Remark 4. (1) While in the case of Theorem 5.1 the restriction $\|\nabla^j \beta\|_{L^\infty} \lesssim (R^{\rm a})^{-j}$ is somewhat significant in that it prevents the "optimal scaling" $R^{\rm b} - R^{\rm a} \approx (R^{\rm a})^{1/3}$ derived in section 2, in the case of the P2-BGFC, the scaling $R^{\rm b} - R^{\rm a} \approx R^{\rm a}$ is in fact required to obtain the optimal rate.

(2) We did not state an energy error estimate, since the analysis of section 5.4 suggests that $(R^{\rm a})^{-2-d}$ is a natural limit, as it is the error rate for the error in the energy itself even without taking into account coarsening (cf. the treatment of T_1 in section 5.4).

6.3. Best approximation operator. Our first ingredient in the convergence proof of P2-BGFC is a new best approximation operator, which is a straightforward modification of the operator constructed in section 4.2.4 of [10].

Let T_R denote the truncation operator defined in [10, eq. (4.20), sect. 4.2.4], and let I_h be the mixed P1/P2 nodal interpolant, defined as follows: Let $\mathcal{E}_h^{(\rm P1)}$ denote the set of edges (*not* faces in three dimensions) of elements $T \in \mathcal{T}_h^{(\rm P1)}$, and let $\mathcal{E}_h^{(\rm P1)}$ denote the remaining edges of the triangulation $\mathcal{T}_h$. Let $\phi_{h,\nu}$ and $\phi_{h,e}$ denote the P2 nodal basis functions associated, respectively, with the nodes $\nu \in \mathcal{X}_h$ and edges $e \in \mathcal{E}_h^{(\rm P2)}$. Let ξ_e denote the edge midpoints, and let $\xi_e^\pm$ denote the two endpoints of each edge. Then for $f \in C(\mathbb{R}^d;\mathbb{R}^d)$,

$$I_h f := \sum_{\xi\in\mathcal{X}_h} f(\xi)\phi_{h,\nu} + \sum_{e\in\mathcal{E}_h^{(\rm P2)}} f(\xi_e)\phi_{h,e} + \sum_{e\in\mathcal{E}_h^{(\rm P1)}} \frac{1}{2}(f(\xi_e^+) + f(\xi_e^-))\phi_{h,e}.$$

Then we define $\Pi_h f := I_h T_{R^c} f$. Following [10, Lem. 4.4, sect. 4.2.4] we immediately obtain

$$\begin{aligned}\|\nabla \Pi_h u^{\mathrm{a}} - \nabla \overline{u^{\mathrm{a}}}\|_{L^2} &\le C\Big(\|h^2 \nabla^3 \tilde{u}^{\mathrm{a}}\|_{L^2(\Omega^{\mathrm{c}})} + \|\nabla \overline{u^{\mathrm{a}}}\|_{L^2(\mathbb{R}^d \setminus B_{R^{\mathrm{c}}/2})}\Big) \\ &\le C\Big((R^{\mathrm{a}})^{-d/2-2} + (R^{\mathrm{c}})^{-d/2}\Big) \le C(R^{\mathrm{a}})^{-d/2-2}, \end{aligned} \tag{6.3}$$

where C depends only on $\mathbf{C}$ and on u^{a}. In the last estimate of (6.3) we used the assumption that $R^{\mathrm{c}} \ge C_\Omega (R^{\mathrm{a}})^{1+4/d}$.

6.4. Proof of Theorem 6.1. The result stated in Theorem 6.1 is an immediate corollary of the following two lemmas, following the strategy of the proof of [10, Thm. 3.1].

LEMMA 6.2 (stability). *Under the conditions of Theorem* 6.1*, let*

$$\gamma^{\mathrm{a}} := \inf_{\substack{v \in \mathscr{U}_0 \\ \|\nabla \bar{v}\|_{L^2}=1}} \langle \delta^2 \mathscr{E}^{\mathrm{a}}(u^{\mathrm{a}}) v, v\rangle > 0 \quad \textit{and} \quad \gamma^{\mathrm{b}} := \inf_{\substack{v_h \in \mathscr{U}_h^{(2)} \\ \|\nabla v_h\|_{L^2}=1}} \langle \delta^2 \mathscr{E}^{\mathrm{bg2}}(\Pi_h u^{\mathrm{a}}) v_h, v_h\rangle.$$

Then, there exists a function $\omega(R) \to 0$ as $R \to \infty$ such that $\gamma^{\mathrm{b}} \ge \gamma^{\mathrm{a}} - \omega(R^{\mathrm{a}})$. Choosing R^{a} sufficiently large guarantees that $\gamma^{\mathrm{b}} \ge \gamma^{\mathrm{a}}/2$.

LEMMA 6.3 (consistency). *Under the assumptions of Theorem* 6.1*, there exists a constant C that depends only on u^{a} and $\mathbf{C}$ such that*

$$\langle \delta \mathscr{E}^{\mathrm{bg2}}(\Pi_h u^{\mathrm{a}}) + \delta \mathscr{P}^{\mathrm{def}}(\Pi_h u^{\mathrm{a}}), v_h\rangle \le C(R^{\mathrm{a}})^{-d/2-2} \|\nabla v_h\|_{L^2} \quad \forall v_h \in \mathscr{U}_h^{(2)}.$$

6.5. Proof of Lemma 6.2: Stability. The corresponding stability result for the P1-BQCE method is [10, Thm. 4.8]. Its proof in [10, sect. 7.1] is lengthy and technical. Since it does not employ the fact that v_h is piecewise affine, with the exception of a short passage in Step 1.1 in the proof of [10, Lem. 10], we shall only give the relevant modification required.

To carry this out, we first recall from the proof of Lemma 4.10 in [10, sect. 7.1] that it is sufficient to assume $u^{\mathrm{a}} = \Pi_h u^{\mathrm{a}} = 0$, $\mathscr{P}^{\mathrm{def}} = 0$. Next, we set $\varepsilon := 1/R^{\mathrm{a}}$ and rescale

$$x \mapsto \varepsilon x, \quad v_h \mapsto \varepsilon^{1-d/2} v_h, \Omega_h \mapsto \varepsilon \Omega_h, \quad \beta \mapsto \beta(\varepsilon^{-1}\cdot).$$

With this rescaling, $\|\nabla v_h\|_{L^2}$ is preserved, and the atomistic and blending regions are now contained within an $O(1)$ domain that is independent of R^{a} (or ε) and $\|\nabla^j \beta\|_{L^\infty} \le C_\beta$, $j = 0, 1, 2$.

The step that must be modified is to replace (in the notation of [10])

$$\int_{\Omega_n} (Q_n \beta_n)(\mathbb{C} : \nabla z_n) : \nabla z_n \,\mathrm{d}x \quad \text{with} \quad \int_{\Omega_n} \beta_n \mathbb{C} : \nabla z_n : \nabla z_n \,\mathrm{d}x,$$

up to a controllable error, where $\mathbb{C} = \partial^2 W(0)$. In our setting we must estimate, for any $z \in \dot{H}^1 := \{z \in H^1_{\mathrm{loc}} \,|\, \nabla z \in L^2\}$,

$$\int_{\Omega_h} Q_h\big[\beta(\mathbb{C} : \nabla z) : \nabla z\big] \,\mathrm{d}x \ge \int_{\Omega_h} \beta(\mathbb{C} : \nabla z) : \nabla z \,\mathrm{d}x - C\varepsilon \|\nabla z\|_{L^2}^2. \tag{6.4}$$

Let Q_0 denote the piecewise constant midpoint interpolant; then using the fact that Q_h integrates quadratics exactly, we obtain

$$\begin{aligned}\int_{\Omega_h} Q_h\big[\beta(\mathbb{C} : \nabla z) : \nabla z\big]\,\mathrm{d}x &\\ &\geq \int_{\Omega_h} Q_h\big[Q_0\beta(\mathbb{C} : \nabla z) : \nabla z\big]\,\mathrm{d}x - C\|\beta - Q_0\beta\|_{L^\infty}\|\nabla z\|_{L^2}^2\\ &= \int_{\Omega_h} Q_0\beta\big[(\mathbb{C} : \nabla z) : \nabla z\big]\,\mathrm{d}x - C\|\beta - Q_0\beta\|_{L^\infty}\|\nabla z\|_{L^2}^2\\ &\geq \int_{\Omega_h} \beta\big[(\mathbb{C} : \nabla z) : \nabla z\big]\,\mathrm{d}x - 2C\|\beta - Q_0\beta\|_{L^\infty}\|\nabla z\|_{L^2}^2.\end{aligned}$$

Since $\|\beta - Q_0\beta\|_{L^\infty} \leq C\varepsilon$ we obtain the required estimate (6.4).

This completes the proof of Lemma 6.2.

6.6. Proof of Lemma 6.3: Second-order consistency. To prove Lemma 6.3 we need to make a small (but nontrivial) modification of the consistency analysis of the standard (P1) BQCE method [10, sect. 6] and combine it with the modifications already made in section 5.3. In the remainder of this subsection let $u \equiv u^{\mathrm{a}}$ and $u_h \equiv \Pi_h u^{\mathrm{a}}$.

To make these modifications, we first review another technical tool from [10]. Recall from section 5.1 the definition of the atomistic lattice P1 interpolant $\bar{v}$ for any $v : \Lambda \to \mathbb{R}^d$. Recall from section 5.3 that $\bar{\zeta}$ is the P1 nodal basis function associated with 0; then $\bar{v} = \sum_{\ell\in\Lambda} v(\ell)\bar{\zeta}(\cdot - \ell)$. In the following analysis we also employ the *quasi-interpolant* $v^* := \bar{\zeta} * \bar{v}$. Properties of the operation $v \mapsto v^*$ are summarized in [10, 20]. In particular, we need that the operation $v \mapsto v^*, \mathscr{U}^{1,2} \to \mathscr{U}^{1,2}$ is an isomorphism [20, Lem. 7].

Following [10, sect. 6], given v_h, we choose $v \in \mathscr{U}_0$ (to be specified in section 6.6.1) satisfying the requirements

$$v(\ell) = v_h(\ell) \quad \forall\, \ell \in \Lambda^{\mathrm{a}} := \cup\mathcal{T}_h^{(\mathrm{P1})} \cap \Lambda \quad \text{and} \quad \|\nabla\bar{v}\|_{L^2} \leq C\|\nabla v_h\|_{L^2}, \tag{6.5}$$

where C may depend only on $\mathbf{C}$. We shall construct v below to satisfy these.

We now define $w \in \mathscr{U}_h$ such that $w^* = v$ (this can be done since the $*$ operator is an isomorphism) and split the consistency error into

$$\begin{aligned}\langle \delta\mathscr{E}^{\mathrm{bg2}}(u_h) + \delta\mathscr{P}^{\mathrm{def}}(u_h), v_h\rangle &= \langle \delta\mathscr{E}^{\mathrm{bg2}}(u_h), v_h\rangle - \langle \delta\mathscr{E}^{\mathrm{a}}(u), w^*\rangle\\ &= \int_{\mathbb{R}^d} Q_h\big[\beta\big(\partial W''(\nabla u_h) - \partial W''(\nabla\tilde{u})\big) : \nabla v_h\big]\,\mathrm{d}x\\ &\quad + \int_{\mathbb{R}^d} \big(Q_h - \mathrm{Id}\big)\big[\beta\partial W''(\nabla\tilde{u}) : \nabla v_h\big]\,\mathrm{d}x\\ &\quad + \int_{\mathbb{R}^d} \beta\partial W''(\nabla\tilde{u}) : \big(\nabla v_h - \nabla\bar{w}\big)\,\mathrm{d}x\\ &\quad + \int_{\mathbb{R}^d} \mathsf{R}^\beta(\tilde{u}) : \nabla\bar{w}\,\mathrm{d}x\\ &=: \mathrm{T}_1 + \mathrm{T}_2 + \mathrm{T}_3 + \mathrm{T}_4,\end{aligned}$$

where

$$\mathsf{R}^\beta(\tilde{u}) = \beta\partial W'' - \sum_{\ell\in\Lambda}\beta(\ell)\sum_{\rho\in\mathcal{R}}\big[V''_{,\rho}\otimes\rho\big]\omega_\rho(\ell - x).$$

The terms $\mathrm{T}_1, \mathrm{T}_2, \mathrm{T}_4$ are estimated analogously as in [10, sect. 6.1] with the modifications from section 5.3; thus, we shall be very brief. Term T_1 can be estimated using (6.3) by

$$|\mathrm{T}_1| \le C(R^{\mathrm{a}})^{-d/2-2}\|\nabla v_h\|_{L^2}. \tag{6.6}$$

Term T_2 is estimated using standard finite element quadrature error estimation techniques by

$$|\mathrm{T}_2| \le C\big\|h^2\nabla^2\big(\beta\partial W(\nabla\tilde{u})\big)\big\|_{L^2}\|\nabla v_h\|_{L^2} \le C(R^{\mathrm{a}})^{-d/2-2}\|\nabla v_h\|_{L^2}, \tag{6.7}$$

where, to obtain the last inequality, we employ the arguments from section 5.3. Term T_4 was already estimated in section 5.3,

$$|\mathrm{T}_4| \le C(R^{\mathrm{a}})^{-d/2-2}\|\nabla v_h\|_{L^2}. \tag{6.8}$$

It is important to note that, up to this point, the choice of v was unimportant as long as it satisfied (6.5).

6.6.1. Estimation of T_3. Only the estimation of T_3 remains. For this term, the techniques from [10] must be modified due to the fact that in the estimation of T_3 in [10, Lem. 6.2, sect. 6.1] only a first-order consistency of this term is obtained. (This was sufficient for [10] as only P1 finite element coarsening is considered.)

Let $f := -\mathrm{div}[\beta\partial W(\nabla\tilde{u})]$; then we split the T_3 further,

$$\begin{aligned}\mathrm{T}_3 &= \int f\cdot(v_h-\bar{w})\,\mathrm{d}x\\ &= \int f\cdot(v_h-\bar{v})\,\mathrm{d}x + \int f\cdot(\bar{v}-\bar{w})\,\mathrm{d}x\\ &=: \mathrm{T}_{3,1}+\mathrm{T}_{3,2}.\end{aligned}$$

To estimate $\mathrm{T}_{3,2}$, we write $\bar{v}-\bar{w} = \sum_{\ell\in\Lambda}(v(\ell)-\bar{w})\bar{\zeta}_\ell$, where $\bar{\zeta}_\ell := \bar{\zeta}(\cdot-\ell)$. The fact that $w^* = v$ means that $\int(v(\ell)-\bar{w})\bar{\zeta}_\ell\,\mathrm{d}x = 0$, which allows us to write

$$\begin{aligned}\int f\cdot(\bar{v}-\bar{w})\,\mathrm{d}x &= \sum_{\ell\in\Lambda}\int f\cdot(v(\ell)-\bar{w})\bar{\zeta}_\ell\,\mathrm{d}x\\ &= \sum_{\ell\in\Lambda}\int (f-\langle f\rangle_{\omega_\ell})\cdot(v(\ell)-\bar{w})\bar{\zeta}_\ell\,\mathrm{d}x\\ &\le \sum_{\ell\in\Lambda}\|f-\langle f\rangle_{\omega_\ell}\|_{L^2(\omega_\ell)}\|v(\ell)-\bar{w}\|_{L^2(\omega_\ell)},\end{aligned}$$

where $\omega_\ell = \mathrm{supp}(\bar{\zeta}_\ell)$. The first term is estimated using Poincaré's inequality, while the second term is estimated from standard quasi-interpolation error estimates (see, e.g., [1]), so we obtain

$$\int f\cdot(\bar{v}-\bar{w})\,\mathrm{d}x \le C\sum_{\ell\in\Lambda}\|\nabla f\|_{L^2(\omega_\ell)}\|\nabla\bar{w}\|_{L^2(\omega_\ell)} \le C\|\nabla f\|_{L^2}\|\nabla\bar{w}\|_{L^2},$$

where in the last line we used the fact that each point in space is covered only by a finite number of patches ω_ℓ. Since $\|\nabla\bar{w}\|_{L^2}\le C\|\nabla\bar{v}\|\le C\|\nabla v_h\|_{L^2}$ we arrive at

$$|\mathrm{T}_{3,2}| \le C\|\nabla f\|_{L^2}\|\nabla v_h\|_{L^2} \le C(R^{\mathrm{a}})^{-d/2-2}\|\nabla v_h\|_{L^2}. \tag{6.9}$$

To estimate $\mathrm{T}_{3,1}$ we must finally face the task of constructing v. The requirement $v(\ell) = v_h(\ell)$, $\ell \in \Lambda^{\mathrm{a}}$, acts like a Dirichlet condition, which motivates the use of a technique in [1] to extend the definition of v to $\Lambda^{\mathrm{c}} := \Lambda \setminus \Lambda^{\mathrm{a}}$: We first decompose $v = v' + z$, where $v'(\ell) = (\bar{\zeta}_\ell * v_h)(\ell)$, $\ell \in \Lambda^{\mathrm{c}}$, $v'(\ell) = v_h(\ell)$, $\ell \in \Lambda^{\mathrm{a}}$, and hence $z(\ell) = 0$ for $\ell \in \Lambda^{\mathrm{a}}$. Next we create a partition of unity $\{\bar{\zeta}_\ell^{\mathrm{PU}} \,|\, \ell \in \Lambda^{\mathrm{c}}\}$ of $\Omega^{(2)} := \mathbb{R}^d \setminus \mathcal{T}_h^{(\mathrm{P1})}$, defined by

$$\bar{\zeta}_\ell^{\mathrm{PU}} := \frac{\bar{\zeta}_\ell}{\sum_{k \in \Lambda^{\mathrm{c}}} \bar{\zeta}_k} \quad \text{for } \ell \in \Lambda^{\mathrm{c}}. \tag{6.10}$$

We then choose the nodal values

$$z(\ell) := \frac{\int_{\Omega^{(2)}} (v_h - \bar{v}') \bar{\zeta}_\ell^{\mathrm{PU}} \,\mathrm{d}x}{\int_{\Omega^{(2)}} \bar{\zeta}_\ell \,\mathrm{d}x}.$$

With this definition v is clearly well-defined, and a much simplified argument of that given in [1] readily establishes (6.5). As a matter of fact, one obtains the stronger result that

$$|z(\ell)| \le C \|v_h - \bar{v}'\|_{L^2(\omega_\ell^{\mathrm{PU}})} \le C \|\nabla v_h\|_{\omega_\ell^{\mathrm{ext}}}, \tag{6.11}$$

where $\omega_\ell^{\mathrm{PU}} = \mathrm{supp}(\bar{\zeta}_\ell^{\mathrm{PU}}) = \omega_\ell$ and $\omega_\ell^{\mathrm{ext}} = \cup_{k \in \Lambda \cap \omega_\ell} \omega_k$.

Using the fact that $v_h = \bar{v}$ in $\cup \mathcal{T}_h^{(\mathrm{P1})}$, and the partition of unity property of $\bar{\zeta}_\ell^{\mathrm{PU}}$, we write

$$\mathrm{T}_{3,1} = \int_{\Omega^{(2)}} f \cdot (v_h - \bar{v}) \,\mathrm{d}x = \sum_{\ell \in \Lambda^{\mathrm{c}}} \int_{\Omega^{(2)}} f \cdot \Big[(v_h - \bar{v}') \bar{\zeta}_\ell^{\mathrm{PU}} - z(\ell) \bar{\zeta}_\ell \Big] \,\mathrm{d}x.$$

Employing (6.10) we can subtract a local average of f over $\omega_\ell^{\mathrm{PU}}$, followed by an application of Poincaré's inequality, the estimate (6.11), and the finite overlap of the patches ω_ℓ, $\omega_\ell^{\mathrm{ext}}$, to conclude that

$$\begin{aligned} |\mathrm{T}_{3,1}| &= \left| \sum_{\ell \in \Lambda^{\mathrm{c}}} \int_{\Omega^{(2)}} \big[f - \langle f \rangle_{\omega_\ell^{\mathrm{PU}}} \big] \cdot \Big[(v_h - \bar{v}') \bar{\zeta}_\ell^{\mathrm{PU}} - z(\ell) \bar{\zeta}_\ell \Big] \,\mathrm{d}x \right| \\ &\le C \|\nabla f\|_{L^2} \|\nabla v_h\|_{L^2}. \end{aligned}$$

Thus, in summary we have proven that

$$|T_3| \le C \|\nabla f\|_{L^2} \|\nabla v_h\|_{L^2} \le C (R^{\mathrm{a}})^{-d/2-2} \|\nabla v_h\|_{L^2}. \tag{6.12}$$

Combining (6.6), (6.7), (6.8), and (6.12) completes the proof of Lemma 6.3.

Conclusion. We introduced a new variation of a/c coupling, BGFC, that combines the benefits of blending [27] and ghost force correction [24]. The construction is performed in such a way that the scheme can be understood as energy-based, whereas other variants of ghost force correction are usually understood as force-based [4].

We described the construction of BGFC for a variety of examples and numerically demonstrated that standard BGFC (with P1-FEM) has optimal rates of convergence, in terms of the number of degrees of freedom, among all a/c couplings employing P1 finite elements in the continuum region. Moreover, we demonstrated that P2-BGFC, employing P2-FEM in the continuum region, has an optimal convergence rate among all a/c couplings employing the Cauchy–Born continuum model.

We also gave rigorous justifications for these statements for a point defect model problem in Theorems 5.1 and 6.1.

REFERENCES

[1] C. Carstensen, *Quasi-interpolation and a posteriori error analysis in finite element methods*, M2AN Math. Model. Numer. Anal., 33 (1999), pp. 1187–1202.

[2] M. S. Daw and M. I. Baskes, *Embedded-atom method: Derivation and application to impurities, surfaces, and other defects in metals*, Phys. Rev. B, 29 (1984), pp. 6443–6453.

[3] A. Dedner, C. Ortner, and H. Wu, work in progress.

[4] M. Dobson and M. Luskin, *Analysis of a force-based quasicontinuum approximation*, M2AN Math. Model. Numer. Anal., 42 (2008), pp. 113–139.

[5] M. Dobson, M. Luskin, and C. Ortner, *Stability, instability, and error of the force-based quasicontinuum approximation*, Arch. Ration. Mech. Anal., 197 (2010), pp. 179–202.

[6] W. E, J. Lu, and J. Z. Yang, *Uniform accuracy of the quasicontinuum method*, Phys. Rev. B, 74 (2006), 214115.

[7] W. E and P. Ming, *Cauchy-Born rule and the stability of crystalline solids: Static problems*, Arch. Ration. Mech. Anal., 183 (2007), pp. 241–297.

[8] V. Ehrlacher, C. Ortner, and A. V. Shapeev, *Analysis of Boundary Conditions for Crystal Defect Atomistic Simulations*, preprint, arXiv:1306.5334v1[math.NA], 2013.

[9] X. H. Li, M. Luskin, C. Ortner, and A. V. Shapeev, *Theory-based benchmarking of blended force-based quasicontinuum method*, Comput. Methods Appl. Mech. Engrg., 268 (2014), pp. 763–781.

[10] X. H. Li, C. Ortner, A. V. Shapeev, and B. Van Koten, *Analysis of Blended Atomistic/Continuum Hybrid Methods*, preprint, arXiv:1404.4878v1[math.NA], 2014.

[11] J. Lu and P. Ming, *Stability of a Force-Based Hybrid Method in Three Dimensions with Sharp Interface*, preprint, arXiv:1212.3643v1[math.NA], 2014.

[12] J. Lu and P. Ming, *Convergence of a force-based hybrid method in three dimensions*, Comm. Pure Appl. Math., 66 (2013), pp. 83–108.

[13] M. Luskin and C. Ortner, *Atomistic-to-continuum-coupling*, Acta Numer., 22 (2013), pp. 397–508.

[14] M. Luskin, C. Ortner, and B. Van Koten, *Formulation and optimization of the energy-based blended quasicontinuum method*, Comput. Methods Appl. Mech. Engrg., 253 (2013), pp. 160–168.

[15] C. Makridakis, C. Ortner, and E. Süli, *A Priori Error Analysis of Two Force-Based Atomistic/Continuum Hybrid Models of a Periodic Chain*, Report 28/2010, OxMOS: New Frontiers in the Mathematics of Solids, Mathematical Institute, University of Oxford, Oxford, UK, 2010.

[16] D. Olson, P. Bochev, M. Luskin, and A. V. Shapeev, *Development of an optimization-based atomistic-to-continuum coupling method*, in Large-Scale Scientific Computing: 9th International Conference (Sozopol, Bulgaria, June 3–7, 2013), Revised Selected Papers, Lecture Notes in Comput. Sci. 8358, Springer, Berlin, 2014, pp. 33–44.

[17] C. Ortner, work in progress.

[18] C. Ortner, *The role of the patch test in* $2D$ *atomistic-to-continuum coupling methods,* ESAIM Math. Model. Numer. Anal., 46 (2012), pp. 1275–1319.

[19] C. Ortner and B. Van Koten. work in progress.

[20] C. Ortner and A. Shapeev, *Interpolants of Lattice Functions for the Analysis of Atomistic/Continuum Multiscale Methods*, preprint, arXiv:1204.3705v1[math.NA], 2012.

[21] C. Ortner and A. V. Shapeev, *Analysis of an energy-based atomistic/continuum approximation of a vacancy in the* $2D$ *triangular lattice*, Math. Comp., 82 (2013), pp. 2191–2236.

[22] C. Ortner and L. Zhang, *Construction and sharp consistency estimates for atomistic/continuum coupling methods with general interfaces: A two-dimensional model problem*, SIAM J. Numer. Anal., 50 (2012), pp. 2191–2236.

[23] C. Ortner and L. Zhang, *Energy-based atomistic-to-continuum coupling without ghost forces*, Comput. Methods Appl. Mech. Engrg., 279 (2014), pp. 29–45.

[24] V. B. Shenoy, R. Miller, E. B. Tadmor, D. Rodney, R. Phillips, and M. Ortiz, *An adaptive finite element approach to atomic-scale mechanics—the quasicontinuum method*, J. Mech. Phys. Solids, 47 (1999), pp. 611–642.

[25] T. Shimokawa, J. J. Mortensen, J. Schiotz, and K. W. Jacobsen, *Matching conditions in the quasicontinuum method: Removal of the error introduced at the interface between the coarse-grained and fully atomistic region*, Phys. Rev. B, 69 (2004), 214104.

[26] B. Van Koten and M. Luskin, *Analysis of energy-based blended quasi-continuum approximations*, SIAM J. Numer. Anal., 49 (2011), pp. 2182–2209.

[27] S. P. Xiao and T. Belytschko, *A bridging domain method for coupling continua with molecular dynamics*, Comput. Methods Appl. Mech. Engrg., 193 (2004), pp. 1645–1669.